Redox Biology 67 (2023) 102906

Contents lists available at ScienceDirect

Redox Biology

journal homepage: www.elsevier.com/locate/redox

Neutrophil extracellular traps drive intestinal microvascular endothelial ferroptosis by impairing Fundc1-dependent mitophagy

Chengnan Chu [a,1], Xinyu Wang [a,1], Chao Yang [a,1], Fang Chen [b], Lin Shi [c], Weiqi Xu [a], Kai Wang [a], Baochen Liu [a], Chenyang Wang [d], Dongping Sun [c], Weiwei Ding [a,*]

[a] Division of Trauma and Acute Care Surgery, Department of Surgery, Jinling Hospital, Affiliated Hospital of Medical School, Nanjing University, Nanjing, Jiangsu Province, China
[b] School of Medicine, Southeast University, Nanjing, 210002, Jiangsu Province, China
[c] Institute of Chemicobiology and Functional Materials, School of Chemistry and Chemical Engineering, Nanjing University of Science and Technology, 200 Xiao Ling Wei Street, Nanjing, 210094, Jiangsu Province, China
[d] Key Laboratory of Intestinal Injury, Research Institute of General Surgery, Affiliated Jinling Hospital, Medical School of Nanjing University, Nanjing, 210002, Jiangsu, PR China

ARTICLE INFO

Keywords:
Intestinal ischemia reperfusion
Neutrophil extracellular traps
Fundc1-dependent mitophagy
Ferroptosis
Microvascular dysfunction

ABSTRACT

Microvascular endothelial damage caused by intestinal ischemia–reperfusion (II/R) is a primary catalyst for microcirculation dysfunction and enterogenous infection. Previous studies have mainly focused on how neutrophil extracellular traps (NETs) and ferroptosis cause intestinal epithelial injury, and little attention has been given to how NETs, mainly from circulatory neutrophils, affect intestinal endothelial cells during II/R. This study aimed to unravel the mechanisms through which NETs cause intestinal microvascular dysfunction. We first detected heightened local NET infiltration around the intestinal microvasculature, accompanied by increased endothelial cell ferroptosis, resulting in microcirculation dysfunction in both human and animal II/R models. However, the administration of the ferroptosis inhibitor ferrostatin-1 or the inhibition of NETs via neutrophil-specific peptidylarginine deiminase 4 (*Pad4*) deficiency led to positive outcomes, with reduced intestinal endothelial ferroptosis and microvascular function recovery. Moreover, RNA-seq analysis revealed a significant enrichment of mitophagy- and ferroptosis-related signaling pathways in HUVECs incubated with NETs. Mechanistically, elevated NET formation induced Fundc1 phosphorylation at Tyr18 in intestinal endothelial cells, which led to mitophagy inhibition, mitochondrial quality control imbalance, and excessive mitochondrial ROS generation and lipid peroxidation, resulting in endothelial ferroptosis and microvascular dysfunction. Nevertheless, using the mitophagy activator urolithin A or AAV-*Fundc1* transfection could reverse this process and ameliorate microvascular damage. We first demonstrate that increased NETosis could result in intestinal microcirculatory dysfunction and conclude that suppressed NET formation can mitigate intestinal endothelial ferroptosis by improving Fundc1-dependent mitophagy. Targeting NETs could be a promising approach for treating II/R-induced intestinal microcirculatory dysfunction.

1. Introduction

Intestinal ischemia–reperfusion (II/R) injury is a serious pathophysiological process that manifests in various clinical conditions, including mesenteric artery occlusion, abdominal trauma, hemorrhagic shock, and intestinal obstruction [1,2]. The intestine, a crucial organ with a substantial blood supply, is susceptible to damage induced by ischemia, hypoxia, and reperfusion. Intestinal microvascular endothelial dysfunction is known to be one of the main causes of gut barrier damage in developing II/R injury [3,4]. At the molecular and cellular levels, increased oxidative stress subsequently causes swelling and vacuolization of endothelial cells, intercellular tight junction loss and hyperpermeability, neutrophil infiltration, and microthrombus formation in the microvasculature [3,5]. Microvascular injury and dysfunction lead to gut barrier damage, which triggers a vicious cycle of aggravating II/R injury [6]. These factors may subsequently lead to the development of

* Corresponding author.
E-mail address: dingwei_nju@hotmail.com (W. Ding).
[1] These authors contributed equally: Chengnan Chu, Xinyu Wang, Chao Yang.

https://doi.org/10.1016/j.redox.2023.102906
Received 14 July 2023; Received in revised form 19 September 2023; Accepted 25 September 2023
Available online 4 October 2023

severe sepsis, septic shock, and even multiple organ dysfunction syndrome (MODS).

Activated neutrophils produce and release neutrophil extracellular traps (NETs), which primarily consist of the extracellular decondensed chromatin with bound histones, myeloperoxidase (MPO), and neutrophil elastase (NE) and are capable of capturing and eliminating infectious microorganisms [7]. While NET components have been identified to have the antimicrobial function, it is important to acknowledge that the dysregulation or excessive formation of NETs may result in a two-sided impact, potentially leading to cellular damage and adjacent tissue injury [8]. Notably, a recent study highlighted the involvement of NETs in the pathogenesis of intestinal, liver, and lung injuries in the context of ischemia–reperfusion (I/R) diseases [9–12]. Interventions aimed at inhibiting NET formation may mitigate ischemia−reperfusion injury in various organs, reduce inflammatory responses, and increase survival rates. Recently, it has been discovered that NETs play a role in the progression of lung and cardiac microvascular damage and microcirculation dysfunction in SARS-CoV-2 infection or myocardial infarction [13,14]. Our prior investigations have established that NETs can potentially impair the intestinal barrier in the aftermath of II/R or sepsis injury [10,15,16]. Nevertheless, the extent to which NET formation may result in intestinal endothelial cell damage and microvascular dysfunction remains largely unexplored.

Mitophagy is a crucial pathway for maintaining mitochondrial homeostasis by sequestering damaged or depolarized mitochondria into autophagosomes for lysosomal degradation. Recent studies have shown that impaired mitophagy may contribute to I/R injury, as the accumulation of defective mitochondria can lead to mitochondrial dysfunction, characterized by ATP synthesis interruption, mitochondrial ROS production, loss of mitochondrial membrane potential, mitochondrial permeability transition pore (mPTP) opening and cytochrome-c (Cytc) leakage [17,18]. The FUN14 domain-containing 1 (Fundc1) protein is an essential component of the mitochondrial outer membrane, which interacts with LC3 to promote mitophagosome formation and maintain proper mitochondrial homeostasis [19]. Fundc1 is believed to have a crucial function in activating mitophagy during ischemic and hypoxic conditions via phosphorylation and dephosphorylation [20]. Furthermore, a recent study demonstrated that NET formation might enhance tumor growth in digestive oncological diseases by impacting mitochondrial homeostasis [21]. However, the role of NET formation in endothelial mitochondrial dysfunction in II/R remains poorly defined. Thus, there is still a strong need to elucidate whether there is a potential link between NET formation, Fundc1-dependent mitophagy regulation, and intestinal microvascular dysfunction, particularly in the context of II/R injury.

Ferroptosis is a new form of iron-dependent regulated cell death resulting from accumulating reactive oxygen species (ROS) and lipid peroxidation. A mounting body of evidence indicates that ferroptosis has a noteworthy influence on chronic and acute gastrointestinal disorders, including acute intestinal ischemia, inflammatory bowel disease, and tumors [4,22,23]. Multiple studies have demonstrated a strong association between mitochondrial dysfunction and ferroptosis, as evidenced by the disruption of ATP synthesis and a subsequent increase in reactive oxygen species (ROS) levels, leading to abnormal iron transport and lipid peroxidation [24,25]. Additionally, morphological changes such as condensed membrane densities, reduced or absent cristae, and outer membrane ruptures have been observed in mitochondria during ferroptosis [26,27]. Although several studies have demonstrated the ability of ferroptosis to induce damage to the intestinal epithelium during II/R conditions [28,29], the relationship between NET formation and ferroptosis, as well as the potential influence of Fundc1-dependent mitophagy on the initiation of ferroptosis in microvascular endothelial cells during II/R, remains unclear.

Herein, we hypothesized that NET formation could trigger intestinal microvascular endothelial ferroptosis by inhibiting Fundc1-dependent mitophagy following II/R conditions. The present study examined the mechanisms underlying NET formation and Fundc1-dependent mitophagy and their influence on ferroptosis in human subjects and an II/R injury model utilizing *Pad4* and *Fundc1* knockout mice. The objective of this investigation was to offer novel insights and therapeutic approaches to the management of microvascular dysfunction during II/R injury.

2. Materials and methods

2.1. Ethics statement

The present investigation was conducted in adherence to the Guidelines for Clinical Trials as recommended by the Ethics Committee of the Jinling Hospital. The study protocol was executed in accordance with the principles outlined in the Declaration of Helsinki and was granted approval by the Ethics Committee of the Jinling Hospital (2022DZGZR-018). Before any study-related procedures, all participants provided written informed consent. The mice were raised in a pathogen-free environment at the Research Institute of General Surgery in Jinling Hospital. They were humanely euthanized through carbon dioxide narcosis in compliance with both local and national ethical guidelines of the use of laboratory animals. The Institutional Animal Care and Use Committee at the Jinling Hospital granted approval for all animal procedures and experimental protocols under reference number 2022DZGKJDWLS-0058.

2.2. Patient recruitment

This study, conducted at the Jinling Hospital (Medical School of Nanjing University, China), included 16 patients diagnosed with isolated acute superior mesenteric artery occlusion disease. Ineffective conservative treatment led to surgical resection of all patients' diseased bowel and intestinal ostomy. The surgical procedures performed were consistent with those described in our previous study [30]. The subsequent analysis involved the collection of eight intestinal samples from resection specimens. The present study utilized healthy intestinal tissues obtained from an intraoperatively removed enterostomy of eight patients who underwent definite intestinal ostomy anastomosis as controls. Additionally, serum samples were collected from all patients before surgery.

2.3. Animal study

Pad4$^{fl/fl}$ C57BL/6 mice (#026708) and Mrp8-Cre (S100A8-Cre) C57BL/6 mice (#021614) were purchased from the Jackson Laboratory (Bar Harbor, ME, USA) through the Model Animals Research Center of Nanjing University as described in our earlier report [15]. *Fundc1*$^{fl/fl}$ C57BL/6 mice and Tie2-Cre (Tek-Cre) C57BL/6 mice were purchased from the Model Animals Research Center of Nanjing University. *Pad4*$^{fl/fl}$ mutant mice were crossed with Mrp8-Cre mice to generate neutrophil-specific *Pad4* knockout (*Pad4*$^{fl/fl}$; Mrp8-Cre, *Pad4*$^{\Delta PMN}$) mice. *Fundc1*$^{fl/fl}$ mice were crossed with Tie2-Cre mice to generate endothelium-specific *Fundc1* knockout (*Fundc1*$^{fl/fl}$; Tie2-Cre, *Fundc1*$^{\Delta EC}$) mice. The Model Animals Research Center of Nanjing University provided WT C57BL/6 mice. Considering estrogen is an independent protective factor against ischemia−reperfusion injury [31,32], male mice aged 8–10 weeks were selected for the study, with five mice allocated to each group. The mice were housed in a controlled environment with regulated light and temperature and were provided ad libitum access to food and water.

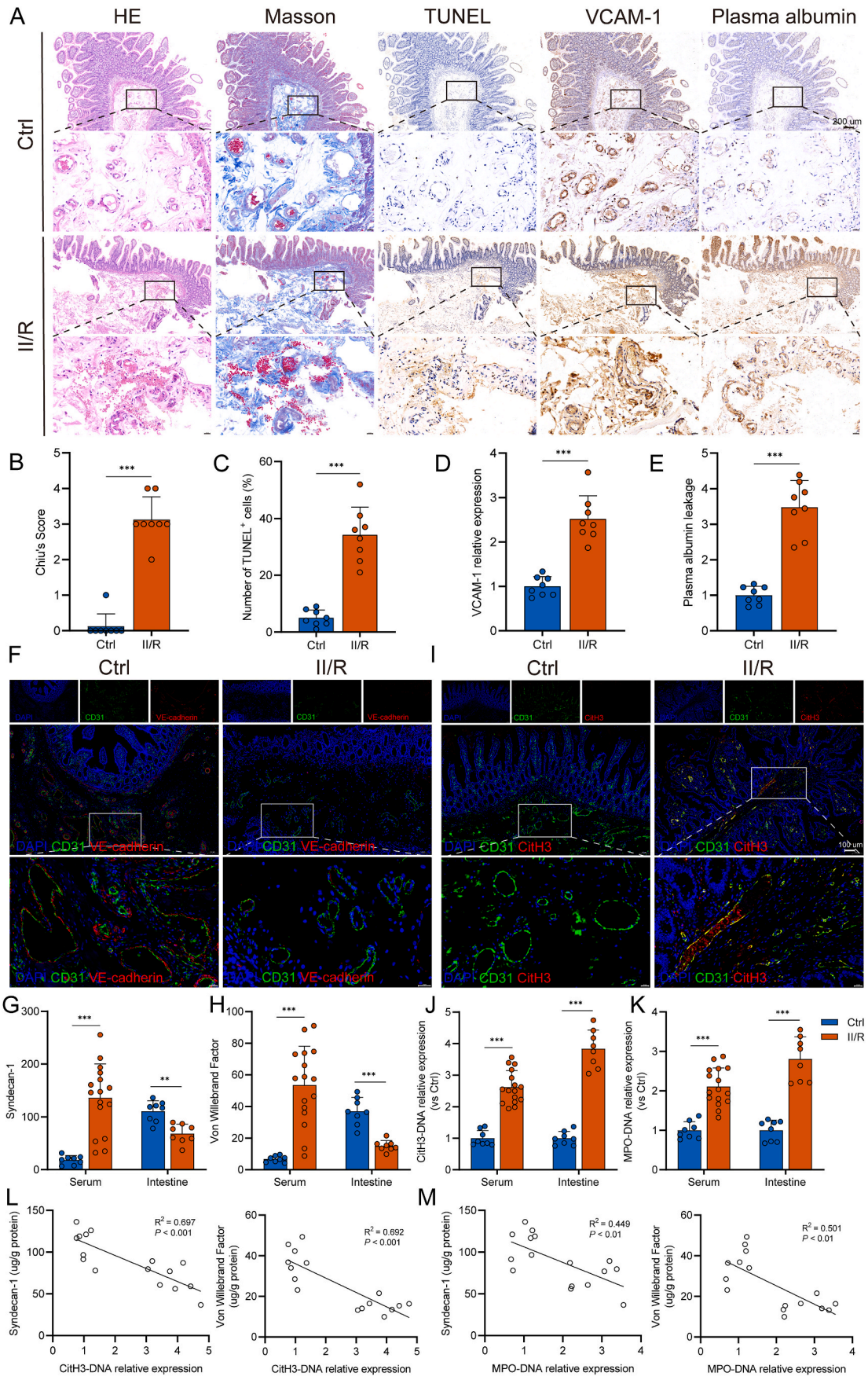

(caption on next page)

Fig. 1. Increased NET levels are associated with intestinal microvascular dysfunction in II/R patients. A–E. Representative photographs showing the pathological changes in the intestine from healthy controls and II/R patients, as observed via microscopy. (B) HE- and Masson's trichrome-stained tissue samples of small bowels were evaluated with the Chiu score system. (C) TUNEL staining was performed to detect apoptosis of intestinal microvascular endothelial cells, and the percentage of TUNEL-positive cells was calculated. (D–E) Immunohistochemical staining for VCAM-1 and albumin was performed in intestinal sections and quantified by the ImageJ software. Scale bars = 200 μm. **F**. Expression levels of CD31 and VE-cadherin (adherens junction protein of the endothelium) were analyzed by immunofluorescence staining. Scale bars = 100 μm. **G**. Syndecan-1 levels in the serum (ng/mL) and intestinal tissue lysates (μg/g protein) were evaluated using ELISA kits. **H**. von Willebrand factor (vWF) concentrations in the serum (ng/mL) and intestinal homogenate (μg/g protein) were evaluated using an ELISA. **I**. Colocalization of intestinal microvascular (CD31) and NET formation (CitH3) was assessed by immunofluorescence staining. Scale bars = 100 μm. **J-K**. Circulating and intestinal MPO-DNA and CitH3-DNA complexes in healthy controls and II/R patients were analyzed by ELISAs. **L-M**. Correlation between intestinal NET biomarkers (CitH3-DNA and MPO-DNA complexes) and intestinal microvascular injury biomarkers (syndecan-1 and vWF). NET, neutrophil extracellular trap; II/R, intestinal ischemia–reperfusion; HE, hematoxylin-eosin; TUNEL, terminal deoxynucleotidyl transferase-mediated dUTP nick-end labeling; VCAM-1, vascular cell adhesion protein 1; CitH3, citrullinated histone H3; MPO, myeloperoxidase. Data are shown as the means ± SD, $^{**}P < 0.01$, $^{***}P < 0.001$.

The II/R model was established according to established protocols outlined in previous literature [29,33]. Briefly, mice were fasted overnight for 12 h, anesthetized with isoflurane (oxygen delivered at 1 L/min with 3% isoflurane for induction and 1.5% isoflurane for maintenance), and placed on the operating table. Following midline laparotomy, II/R injury was induced through the occlusion of the superior mesenteric artery using a nontraumatic vascular clamp for 1 h, followed by 24 h of reperfusion. The animals were promptly revived from anesthesia within 10 min of the surgical procedure and were administered ibuprofen (200 mg/L drinking water) for postoperative analgesia. Additionally, they were closely monitored for 24 h. After reperfusion, the animals were euthanized per the aforementioned protocol, and serum and terminal ileum specimens were collected.

To evaluate the effect of ferroptosis regulation, mice received the ferroptosis activator erastin (15 μg/g, i.p., qd, HY-15763, MCE, China) or the ferroptosis inhibitor ferrostatin-1 (5 μg/g, i.p., qd, HY-100579, MCE, China) for 7 days (Suppl. Fig. 1A) [29,34]. An equal amount of the vehicle (corn oil, HY-Y1888, MCE, China) was delivered to the sham group. To examine the role of mitophagy in II/R, mice received the mitophagy activator urolithin A (UA, 50 μg/g, i.g., qd, HY-100599, MCE, China) or the mitophagy inhibitor mitochondrial division inhibitor 1 (Mdivi-1, 50 μg/g, i.p., qd, HY-15886, MCE, China) for 14 days (Suppl. Fig. 3A) [35–37]. The sham group was given an equal amount of the vehicle (normal saline).

2.4. Histology, immunohistochemistry and immunofluorescence

Fresh terminal ileal tissue specimens were fixed in 4% paraformaldehyde for histological analysis and subsequently embedded in paraffin. Standard hematoxylin and eosin (H&E) staining and Masson's trichrome staining were conducted on the intestinal paraffin sections. Two pathologists employed the Chiu scoring system to evaluate the sections [38].

The tissues were fixed, embedded, and sectioned for immunohistochemistry as previously described. Subsequently, primary antibodies, namely, anti-VCAM1 (ab215380, Abcam, USA) and anti-albumin (66051-1-Ig, Proteintech, China), were added and allowed to incubate overnight at 4 °C after antigen repair. Following incubation with the primary antibodies and an HRP-conjugated secondary antibody, DAB was used as a chromogen. Finally, the sections were visualized after counterstaining with hematoxylin. In addition, TUNEL staining was carried out using a TUNEL apoptosis kit (G1507-100T, Servicebio, China) following the manufacturer's protocol. Analysis was performed using the ImageJ software by investigators who were blinded to the experimental groups.

For immunofluorescence, slides were blinded using 3% BSA for 1 h, followed by overnight incubation at 4 °C with primary antibodies. The primary antibodies included anti-CD31 (human: ab76533; mouse: ab222783, Abcam, USA), anti-VE cadherin (ab33168, Abcam, USA), anti-CitH3 (ab5103, Abcam, USA), anti-Drp1 (ab184247, Abcam, USA), and anti-Tom20 (ab186735, Abcam, USA). The nuclei were subsequently counterstained with DAPI (D1306, Thermo Fisher, USA) in accordance with the manufacturer's instructions. Cells were then captured using a confocal microscope (Nikon Eclipse Ti; Nikon, Japan), while tissue sections were photographed using a fluorescence microscope (IXplore Standard; Olympus, Japan). Two independent investigators analyzed The relative fluorescence intensity using the ImageJ software.

2.5. Enzyme-linked immunosorbent assay (ELISA)

The levels of human syndecan-1 (CSB-E14983h, CusaBio, China), mouse syndecan-1 (CSB-EL020888MO, CusaBio, China), human von Willebrand factor (vWF, CSB-E08437h, CusaBio, China), MDA (S0131 M, Beyotime, China), GSH and GSSG (S0053, Beyotime, China), and Fe^{2+} (BC5415, Solarbio, China) in serum, intestinal tissue or isolated intestinal microvascular endothelial cells were analyzed using commercial ELISA kits according to the manufacturers' protocols.

2.6. Quantification of NETs

Detection and quantification of soluble NETs in human and mouse sera and intestines were accomplished using a CitH3-DNA or MPO-DNA complex ELISA, according to our prior study [15]. Specifically, 96-well plates were coated with anti-CitH3 (ab5103, Abcam, USA) or anti-MPO (ab272101, Abcam, USA) antibodies overnight at 4 °C, followed by blocking with 2% BSA at room temperature for 2 h. Samples were subjected to three washes before being introduced into the wells containing an incubation buffer supplemented with a peroxidase-labeled anti-DNA monoclonal antibody (Cell Death ELISA^{PLUS}, 11774425001, Roche, Switzerland). Following a 2-h incubation, the plates underwent three additional washes. The ABTS peroxidase substrate was then introduced, and the absorbance was measured using a microplate reader (FilterMax 3, Molecular Devices, USA) at 405 nm. The values for soluble NET formation were expressed as a percentage increase in the absorbance above the control.

2.7. Intestinal laser speckle perfusion imaging

An RFLSI Pro Laser Speckle Flow Imaging System (RFSLI ZW/RFLSI III, RWD, China) was used for real-time imaging of intestinal blood perfusion. The mouse terminal ileum and mesangium were positioned externally on a sterilization workstation after 24 h of modeling. Subsequently, the intestinal tract was moistened with physiological saline at 37 °C, and the probe was placed above the intestinal tract. A 785 nm laser wavelength was selected to record microcirculation hemodynamic indicators, including blood flow velocity and tissue perfusion volume.

2.8. Transmission electron microscopy (TEM)

The microvasculature, mitochondrial morphology, and mitophagosomes from intestinal endothelial cells were examined by TEM (Hitachi H-600, Japan). Intestinal tissues were initially fixed with 4% glutaraldehyde and treated with 2% osmium tetroxide. Following dehydration through a series of graded ethanol solutions, the samples were embedded in epoxy resin and sectioned. The thin sections were stained with uranyl acetate and lead citrate to facilitate TEM observations.

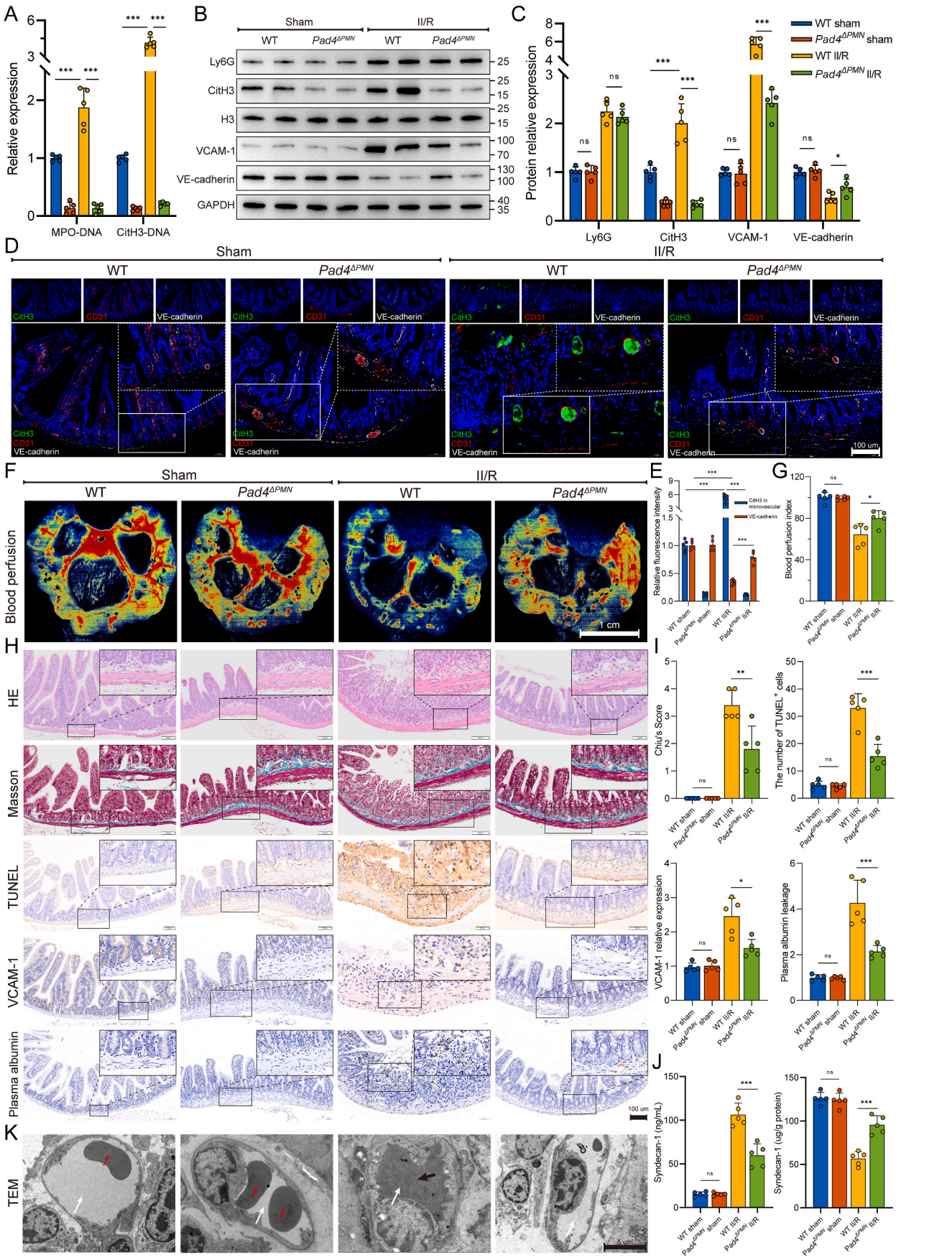

(caption on next page)

Fig. 2. Neutrophil-specific *Pad4* deficiency attenuated intestinal endothelial damage and microvascular dysfunction. A. Intestinal NET biomarkers, CitH3-DNA and MPO-DNA complexes, were measured by ELISAs. **B–C**. Protein expression levels of neutrophil infiltration (Ly6G), NET formation (CitH3) and microvascular damage (VCAM-1 and VE-cadherin) biomarkers were measured by western blotting. The grayscale value of each band was analyzed using the ImageJ software. **D-E**. Immunofluorescent colocalization was performed to assess NET formation (CitH3) in microvascular (CD31) and endothelial (VE-cadherin) injury. Scale bars = 100 μm. **F-G**. Intestinal blood flow and perfusion indices were measured using a laser speckle blood flow analysis system. Scale bars = 1 cm. **H–I**. Intestinal tissue of mice was collected for pathological analysis and immunohistochemical staining. The Chiu score system was employed to evaluate HE- and Masson's trichrome-stained tissue samples from the intestine. To detect apoptosis of intestinal microvascular endothelial cells, TUNEL staining was conducted, and the percentage of TUNEL-positive cells was calculated. Additionally, immunohistochemical staining of VCAM-1 and albumin in intestinal sections was quantified using the ImageJ software. Scale bars = 100 μm. **J**. Expression of syndecan-1 in the serum and intestinal tissues was examined using ELISA kits. **K**. Microvascular and endothelial micromorphological changes were observed by transmission electron microscopy (TEM). Following II/R injury in WT mice, irregular swelling of the endothelium and luminal stenosis were observed in intestinal microvessels, along with the presence of microthrombosis. White arrows denoting the lumen, black arrows indicating the presence of microthrombosis, and red arrows highlighting the presence of red blood cells within the lumen. Data are shown as the means ± SD, ns, not significant, $^{*}P < 0.05$, $^{**}P < 0.01$, $^{***}P < 0.001$.

2.9. NET isolation and cell culture

The methodology utilized to isolate human neutrophils was based on previously established protocols [15,39]. Informed consent was obtained from healthy volunteers, and 5 mL of EDTA-anticoagulated peripheral blood was layered on Polymorphprep (Axis-Shield, Oslo, Norway) and centrifuged for 30 min at 500×*g*. The resulting lower layer containing neutrophils was collected and subsequently washed with phosphate-buffered saline (PBS). Following centrifugation (450×*g*, 5 min), red blood cells were lysed using RBC lysis buffer (Solarbio, Beijing, China). Subsequently, isolated neutrophils were suspended in RPMI 1640 medium (11875-093, Gibco, USA) supplemented with 1% HEPES buffer (15630-080, Gibco, USA). Freshly isolated neutrophils were then seeded in 6-well culture plates at a concentration of 3×10^6 cells per well and stimulated with PMA (100 nM, P1585, Sigma–Aldrich). Following incubation, each well was thoroughly washed twice with 1 mL of PBS, and the content was subsequently resuspended in DMEM (17-207-CV, Corning, USA). The resulting suspension was then centrifugated to eliminate whole cells and debris. After centrifugation, the supernatant was collected and reserved. The quantification of isolated NETs was conducted by assessing the DNA concentration using the Quant-iT™ PicoGreen™ dsDNA Assay kit (P11496, Thermo Fisher, USA).

Human umbilical vein endothelial cells (HUVECs) were procured from the Cell Bank of the Chinese Academy of Sciences (Shanghai, China) and cultured in DMEM (10-013-CVR, Corning, China) supplemented with 10% FBS (10099-141, Gibco, USA). The isolated NETs were diluted in DMEM to achieve a 500 ng/mL concentration. HUVECs were then incubated with either NETs or solvent vehicles for 24 h, after which RNA was extracted and subjected to sequencing.

2.10. RNA sequencing and data analysis

RNA sequencing was conducted on HUVECs that were incubated with or without NETs. The TRIzol reagent (15596026, Invitrogen, USA) was used to extract the total RNA from each sample. The RNA libraries were sequenced on an Illumina sequencing platform (Gene Denovo Biotechnology Co., Ltd., Guangzhou, China). The original gene expression levels were normalized to fragments per kilobase of transcript per million mapped reads (FPKM). The FPKM data elucidated the interrelationship between samples through principal component analysis (PCA) and hierarchical clustering analyses. Differentially expressed genes (DEGs) were determined by applying edgeR general filtering criteria ($|\log_2$ fold change$| > 1.5$, $P < 0.05$) to the FPKM values. Additionally, KEGG and GO annotations were used to identify the relevant pathways of the DEGs.

2.11. Intestinal endothelial cell isolation

Intestinal endothelial cells were isolated and purified through magnetic-activated cell sorting (MACS) utilizing CD31 MicroBead kits (human: 130-091-935; mouse: 130-097-418, Miltenyi Biotec, Germany) in accordance with the manufacturer's instructions. The fresh intestinal specimens obtained during surgery were placed in a cold PBS solution, and any residual intestinal contents and blood cells were rinsed off. The tissue was then cut into small pieces and incubated with an equal volume of 0.5% collagenase type I (SCR103, Sigma, USA) for 45 min. A filter screen was used to eliminate cell clumps, followed by adding red blood cell lysis buffer (BL503B, Biosharp, China) to eliminate red blood cells. Precipitates were collected by centrifugation, and the cells were resuspended in DMEM. Total cell number was assessed using a cell counter (IC 1000, Countstar BioTech, China). CD31 magnetic beads were introduced to system (1×10^8 total cells per sample) and incubated at 4 °C for 15 min. The separation column was then fixed in the MACS magnetic field and rinsed with bubble-free buffer; the labeled cell suspension was added to the separation column. The separation column was removed from the magnetic field, followed by adding a buffer solution, and pressure elution was performed to collect the eluted CD31-positive cells. The collected cells were resuspended in an endothelial cell medium (ECM, YZ-1001, Solarbio, China) to facilitate the detection of indicators related to mitophagy and ferroptosis in subsequent analyses.

2.12. Quantitative real-time PCR analysis

Intestinal tissue was subjected to RNA extraction using the TRIzol reagent (15596026, Invitrogen, USA) in accordance with the manufacturer's instructions. The purity and concentration of the extracted RNA were determined using a NanoDrop instrument (Agilent Technologies, USA). Subsequently, single-strand cDNA was synthesized via reverse transcription using the HiScript II QRT SuperMix for qPCR (R223-01, Vazyme, China) according to the manufacturer's instructions. Finally, relative quantification was conducted by real-time PCR using the ChamQ SYBR Color qPCR Master Mix (Q431-02, Vazyme, China) and a Fast 7500 real-time PCR system (Applied Biosystems, USA). The $2^{-\Delta\Delta CT}$ method was used to calculate fold changes in target expression levels, with GAPDH as the endogenous reference. The qRT–PCR primers employed in this study were synthesized by Sangon Biotech (Shanghai, China) and are listed below: Human_*GPx4* Forward: 5′-GACACCGTCTC TCCACAGTTC-3′, Human_*GPx4* Reverse: 5′-CAGGTCCTTCTCTATCAC-CAGG-3′, Human_*ACSL4* Forward: 5′-TCCTTTTTGCGAGCTTTCCGA-3′, Human_*ACSL4* Reverse: 5′-AAGCCGACAATAAAGTACGCAA-3′, Human_*GAPDH* Forward: 5′-CAGGAGGCATTGCTGATGAT-3′, Human_-*GAPDH* Reverse: 5′-GAAGGCTGGGGCTCATTT-3'.

2.13. Mitochondrial extraction

To isolate mitochondria and extract mitochondrial proteins, mitochondrial extraction kits (tissues: C3606, cells: C3601, Beyotime, China) were used according to the manufacturer's protocols. Briefly, cells or tissues were resuspended in 800 μL of the Mitochondria Isolate Reagent, followed by incubation on ice for 15 min and homogenization using a homogenizer. The homogenate was then subjected to centrifugation at 4 °C for 5 min at 600×*g*, followed by transferring the supernatant to a

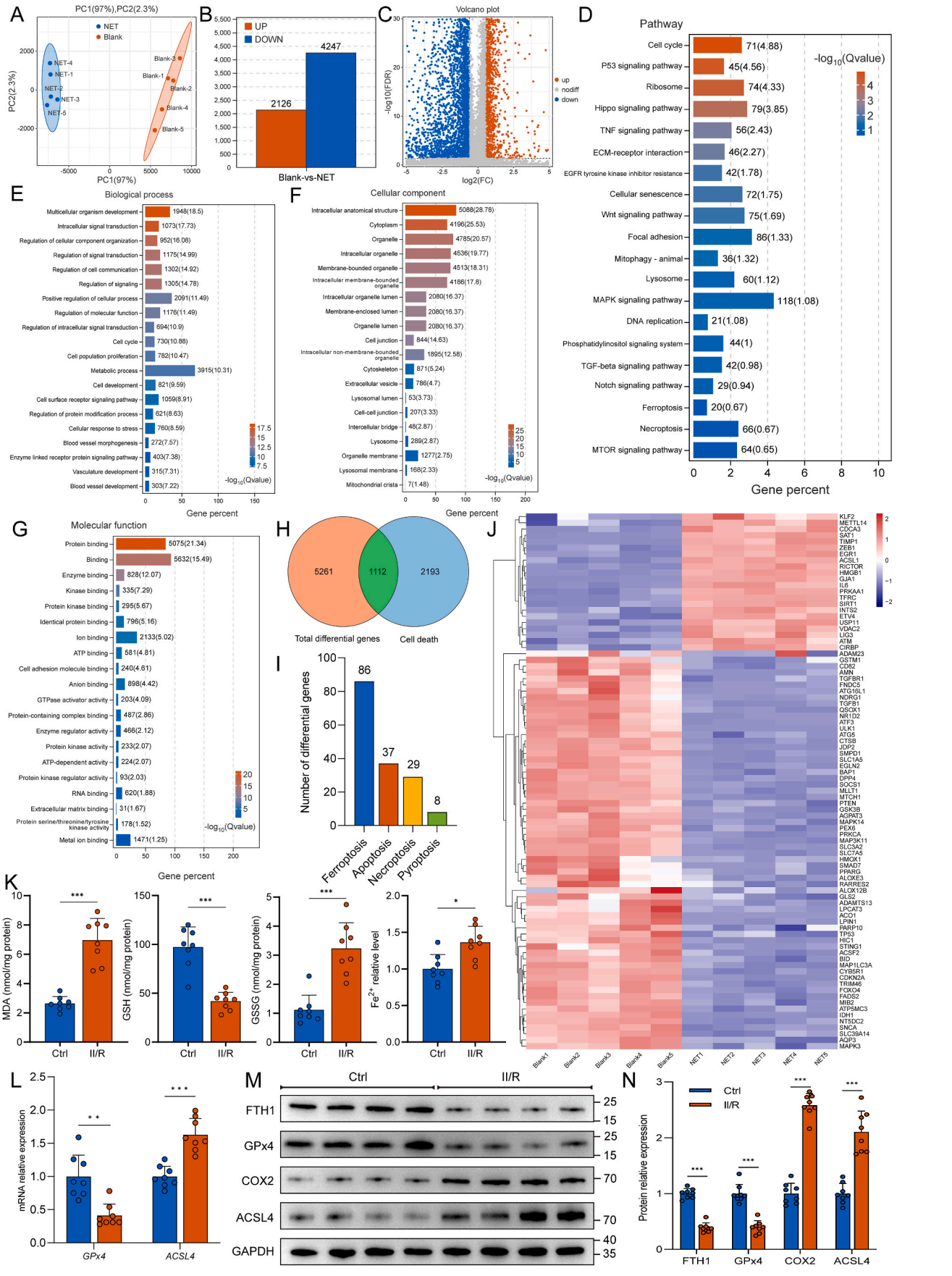

(caption on next page)

Fig. 3. NET formation triggers endothelial ferroptosis in the intestinal microvasculature. HUVECs were cultured in the presence or absence of isolated NETs at a concentration of 500 ng/mL for 24 h. Subsequently, RNA sequencing was conducted on the total RNA extracted from the samples. **A**. PCA was conducted to compare the effects of Blank and NET, which resulted in a distinct separation between the two groups. **B–C**. Bar graph and volcano plot showing differential gene expression between the Blank and NET treatment groups. **D**. KEGG pathway enrichment analysis was performed on differentially expressed genes. **E-G**. GO enrichment analysis of differentially expressed genes was performed to identify significantly enriched GO terms. Panels (E–G) represent BP, CC and MF, respectively. **H**. Comparative analysis between differentially expressed genes and programmed cell death-related genes was conducted using the Gene Ontology (GO) database (http://www.geneontology.org/), and the results are depicted using Venn diagrams. **I**. Bar diagram illustrating the variations in gene expression across various programmed cell death modes. The highest number of differentially expressed genes was found to be associated with ferroptosis. **J**. Heatmap depicting differentially expressed ferroptosis-related genes. **K**. Intestinal endothelial cells were isolated from healthy controls and II/R patients using CD31 magnetic beads. The levels of MDA, GSH, GSSG and Fe^{2+} in the endothelium were determined using ELISAs. **L**. Expression of *GPx4* and *ACSL4* mRNA was measured by real-time PCR. **M-N**. Expression levels of ferroptosis-related proteins in intestinal endothelial cells from healthy controls and II/R patients were tested by western blotting. The grayscale values of the bands were determined using ImageJ. PCA, principal component analysis; KEGG, Kyoto Encyclopedia of Genes and Genomes; GO, Gene Ontology; BP, biological process; CC, cellular component; MF, molecular function; MDA, malondialdehyde; GSH, glutathione; GSSG, glutathione (oxidized); GPx4, glutathione peroxidase 4; ACSL4, acyl-CoA synthetase long chain family member 4. Data are displayed as the mean values with SD, ns, not significant, $^{*}P < 0.05$, $^{**}P < 0.01$, $^{***}P < 0.001$.

fresh tube and subsequent centrifugation (11,000×*g*, 10 min) to pellet mitochondria. The resulting cytosolic supernatant was used for Western blot analysis, while the mitochondrial pellet was washed with cold PBS and resuspended in RIPA lysis buffer for western blotting.

2.14. Fluorescence staining

LysoTracker™ Red (L7528, Thermo Fisher, USA) and MitoTracker™ Green (M7514, Thermo Fisher, USA) were used to track lysosomes and mitochondria, respectively, following the manufacturer's instructions. Intracellular Fe^{2+} was detected using a FerroOrange fluorescent probe (F374, DojinDo, Japan), and nuclei were subsequently counterstained with Hoechst 33342 (C1029, Beyotime, China). Cells were imaged using a confocal microscope (Nikon Eclipse Ti; Nikon, Japan).

2.15. Mitochondrial membrane potential (ΔΨm) detection

The JC-1 assay kit (C2003S, Beyotime, China) was used to measure the mitochondrial membrane potential in accordance with the manufacturer's guidelines. Specifically, cells were incubated for 20 min with the JC-1 staining solution at 37 °C, followed by two washes with the JC-1 buffer solution. JC-1 aggregates and monomers were visualized and captured using a confocal microscope (Nikon Eclipse Ti; Nikon, Japan) with excitation and emission wavelengths of 525 and 590 nm and 490 and 530 nm, respectively.

2.16. ATP generation assessment

The generation of intracellular ATP was assessed using an ATP measurement kit (S0027, Beyotime, China). Following cell harvesting, lysis, and centrifugation, the supernatant was collected and mixed with an ATP detection working solution (100 μL per well) in 96-well plates. Subsequently, samples or ATP standards (20 μL) were added for the detection using a luminometer (FilterMax 3, Molecular Devices, USA). The ATP concentration in each sample was determined by a standard curve.

2.17. Intracellular and mitochondrial ROS detection

Intracellular ROS (cyto-ROS) were quantified using the ROS-sensitive dye DCFH-DA (E004-1-1, Jiancheng, China). Mitochondrial ROS (mito-ROS) and superoxide were measured using the MitoSOX Red mitochondrial superoxide indicator (M36008, Thermo Fisher, USA). The concentrations of cyto-ROS and mito-ROS were determined using a confocal microscope (Nikon Eclipse Ti; Nikon, Japan) in accordance with the manufacturer's instructions.

2.18. Adeno-associated virus (AAV)-mediated gene transfer

To achieve endothelium-specific knockdown of Fundc1, the *Fundc1* shRNA sequence (Target: 5′-GAAGACACCACTGGTGGAATC-3′) was incorporated into an AAV9-TIE1 construct that contained the sequence of TIE1, an endothelial-specific promoter (GeneChem, Shanghai, China). To induce the overexpression of Fundc1 in the endothelium, a cDNA encoding the *Fundc1* sequence, an enhanced GFP reporter gene, and the endothelial-specific TIE1 promoter were generated and inserted into the AAV9 packaging vector (AAV9-TIEp-FUNDC1-EGFP-3Flag-SV40 PolyA). An AAV9 vector that solely expressed the green fluorescent protein served as the negative control (Sh-NC and AAV-NC). The administration protocols were conducted in accordance with prior research [40,41]. Briefly, 1×10^{12} vector genomes (v.g) of AAV9 were injected into the tail veins of mice in 200 μl of PBS 14 days prior to modeling.

2.19. Western blotting

Proteins were extracted from intestinal tissue or cells using a lysis buffer (SD001, Invent Biotechnologies, USA), followed by separation via SDS−PAGE and transfer onto polyvinylidene difluoride membranes (ISEQ00010, Merck Millipore, Ireland). The membranes were subsequently blocked with 5% skim milk for 2 h and incubated with the appropriate primary antibodies overnight at 4 °C. Next, the membranes were incubated with an HRP-conjugated secondary antibody, and protein bands were detected using enhanced chemiluminescence (ECL) luminous fluid (P10300, NCM Biotech, China). The band intensities were analyzed using the ImageJ software. The following primary antibodies were used: Ly6G (1:1000, 87048S, CST, USA), CitH3 (1:2000, ab281584, Abcam, USA), H3 (1:2500, ab1791, Abcam, USA), VCAM-1 (1:1000, ab134047, Abcam, USA), VE-cadherin (1:1000, ab33168, Abcam, USA), GAPDH (1:5000, ab181602, Abcam, USA), FTH1 (1:1000, Mouse: ab183781, Human: ab75972, Abcam, USA), GPx4 (1:1000, ab125066, Abcam, USA), ACSL4 (1:1000, ab155282, Abcam, USA), COX2 (1:1000, ab179800, Abcam, USA), p62 (1:1000, 5114S, CST, USA), LC3 A/B (1:1000, 4108S, CST, USA), Tom20 (1:5000, 11802-1-AP, Proteintech, China), Tim23 (1:1000, 11123-1-AP, Proteintech, China), Cytc (1:1000, DF6457, Affinity, China), VDAC1 (1:1000, ab15895, Abcam, USA), Mfn1 (1:1000, ab126575, Abcam, USA), Opa1 (1:1000, ab157457, Abcam, USA), Opa1 (1:1000, ab157457, Abcam, USA), p-Mff (1:1000, AF14488, Afantibody, China), t-Mff (1:1000, 84580S, CST, USA), Drp1 (1:1000, ab184247, Abcam, USA), and Fundc1 (1:1000, ab224722, Abcam, USA). Rabbit antibodies against p^{Ser17}-Fundc1 and p^{Tyr18}-Fundc1 (1:500) were custom made by Abgent (Suzhou) according to a previous study [42,43].

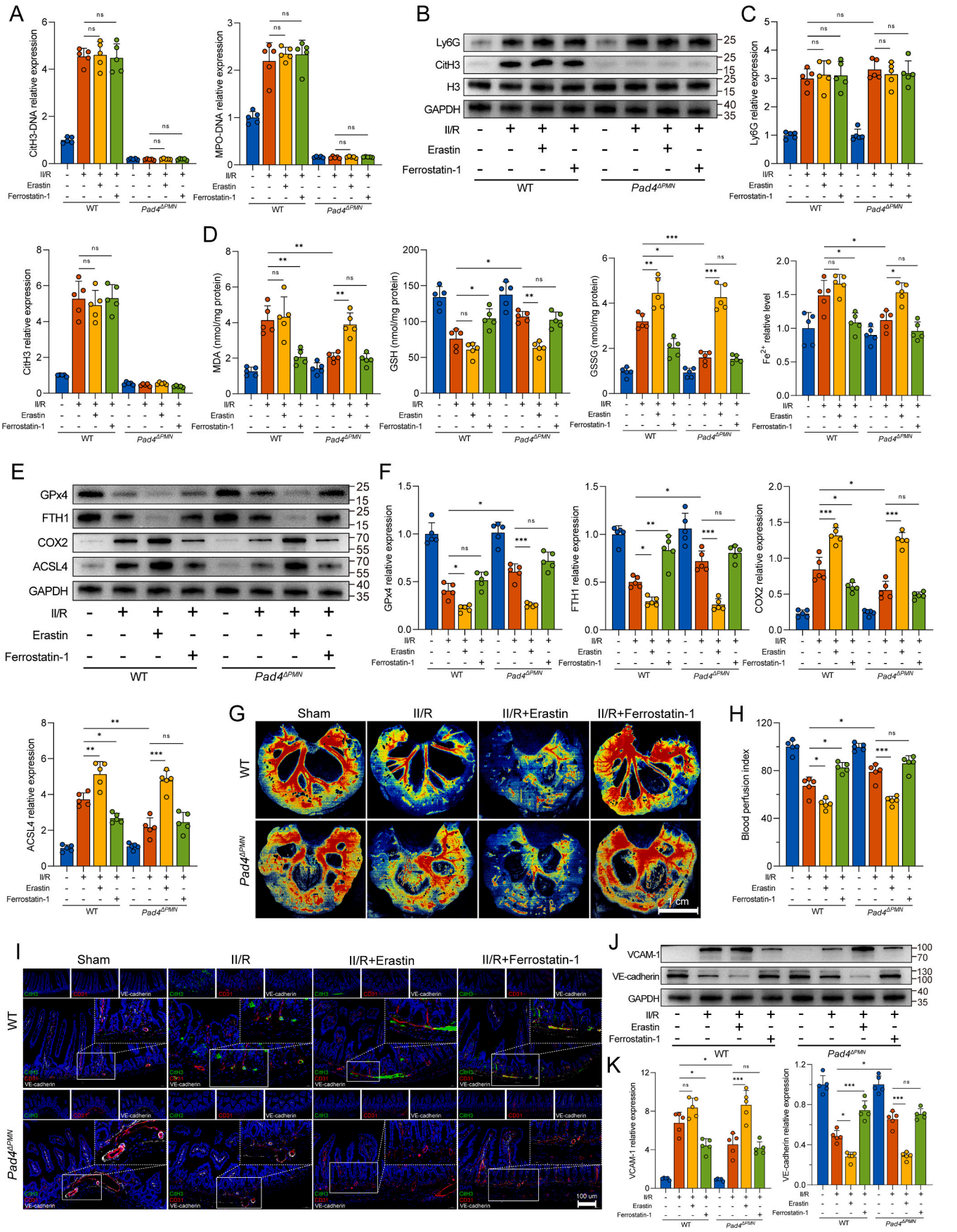

(caption on next page)

Fig. 4. Targeted regulation of ferroptosis has an impact on NET-induced intestinal microvascular dysfunction. A. CitH3-DNA and MPO-DNA complexes in the intestine were measured by ELISAs. **B–C**. Western blotting was used to determine the protein expression levels of Ly6G (neutrophil infiltration) and CitH3 (NET formation). **D**. Intestinal endothelial cells were isolated from WT and *Pad4*$^{\Delta PMN}$ mice using CD31-coated magnetic beads. The intracellular levels of MDA, GSH, GSSG, and Fe^{2+} were analyzed by ELISAs. **E-F**. Ferroptotic protein levels in the intestinal endothelium were evaluated using western blotting. The grayscale values of the bands were determined using ImageJ. **G-H**. Intestinal blood flow and perfusion indices were measured with a laser speckle blood flow imager. **I**. Assessment of NET formation (CitH3) in microvascular (CD31) and endothelial (VE-cadherin) injury was conducted using immunofluorescent colocalization. Scale bars = 100 μm. **J-K**. Western blot quantification of the intestinal microvascular damage markers VCAM-1 and VE-cadherin. Grayscale images were then analyzed using ImageJ. All the data are expressed as the means ± SD, ns, not significant, $^{*}P < 0.05$, $^{**}P < 0.01$, $^{***}P < 0.001$.

2.20. Statistical analysis

Statistical analyses were conducted using GraphPad Prism version 9.31 (GraphPad Software, Inc., La Jolla, CA). The data are presented as either the mean ± standard deviation (SD) or the median with an interquartile range. The normal distribution and homogeneity of variance were assessed for all variables using the Shapiro−Wilk and Levene tests, respectively. In the case of clinical samples, the *t*-test was employed for normally distributed data, while nonnormally distributed data were evaluated using the Wilcoxon test. In the context of mouse and cell studies, statistical analysis was conducted using one or two-way ANOVA for experiments involving one or two factors and three-way ANOVA for experiments involving three factors. Subsequently, a post-hoc Tukey's test was performed. Statistical significance was determined by a *P* value of less than 0.05 ($^{*}P < 0.05$, $^{**}P < 0.01$, $^{***}P < 0.001$).

3. Results

3.1. Increased intestinal microvascular injury and NET formation in II/R patients

We first performed hematoxylin–eosin and Masson's trichrome staining to evaluate the histopathological changes and inflammatory cell infiltration in intestinal tissue. The II/R group presented with microvascular dilation, erythrocyte stasis, thrombus formation, and neutrophil infiltration near the vessel wall, and a higher Chiu score in the intestine (Fig. 1A and B). TUNEL staining indicated that more vascular endothelial cells underwent apoptosis in response to II/R injury (Fig. 1A and C). Vascular cell adhesion molecule 1 (VCAM-1), a surface marker characteristic of vascular endothelial dysfunction, was found to be upregulated in response to vascular injury. In parallel, immunohistochemical staining showed higher expression of VCAM-1, circumscribing the intestinal microvasculature, in II/R patients than in controls (Fig. 1A and D). As shown in Fig. 1A and E, II/R also induced more plasma albumin leakage from the vessel wall into the intestinal interstitial spaces, indicating an elevation in microvascular permeability following II/R injury. Moreover, the results showed that II/R injury led to the downregulation of VE-cadherin, a crucial junctional protein sustaining microvascular permeability, as supported by immunofluorescence analysis (Fig. 1F). In addition, the serum levels of syndecan-1 and von Willebrand factor (vWF) were increased in II/R patients compared to those in healthy controls (Fig. 1G and H). In contrast, significantly lower levels of these factors were observed in the intestinal tissues of II/R patients.

Our previous studies have reported NET formation in intestinal tissue [15,16]; hence, we first sought to investigate the connection between NETs and intestinal microvascular injury during II/R. As shown in Fig. 1I, immunofluorescence colocalization of CD31 and CitH3 confirmed the abundant formation and infiltration of NETs in the intestinal microvasculature of II/R patients. Meanwhile, the levels of CitH3-DNA and MPO-DNA complexes, which are specific biomarkers of NETs, were significantly elevated in both the serum and intestinal tissue of patients with II/R (Fig. 1J and K). Moreover, there were significant correlations between NET biomarkers and microvascular damage markers in the intestine (Fig. 1L and M). These results show a solid association between NET formation and intestinal microvascular injury during II/R in humans.

3.2. Pad4 deficiency ameliorated intestinal microvascular dysfunction in mice

Peptidylarginine deiminase 4 (PAD4) is a histone-modifying enzyme highly expressed in neutrophils and crucial for NET formation. Therefore, neutrophil-specific *Pad4* (*Pad4*$^{\Delta PMN}$) knockout mice were used to investigate the connection between NET formation and intestinal microvascular injury. As shown in Fig. 2A, *Pad4* deficiency led to lower formation of intestinal NET biomarkers (MPO-DNA and CitH3-DNA complexes) after II/R. WB analysis revealed no obvious difference in intestinal Ly6G expression between WT II/R and *Pad4*$^{\Delta PMN}$ II/R mice (Fig. 2B and C), indicating that *Pad4*$^{\Delta PMN}$ deficiency did not affect neutrophil infiltration. However, the CitH3 expression level in the *Pad4*-deficient intestine was markedly decreased during II/R, accompanied by increased VCAM-1 and reduced VE-cadherin protein levels. Likewise, II/R increased CitH3 expression in intestinal microvessels, along with decreased expression of VE-cadherin, and these effects were reversed by the *Pad4* deletion (Fig. 2D and E). Subsequently, laser speckle flowmetry was used to functionally assess intestinal blood perfusion. The results showed that the intestinal blood perfusion index was significantly decreased in II/R-treated mice, while *Pad4* deficiency sustained blood flow perfusion (Fig. 2F and G). To analyze the pathological impairment of the intestinal microvasculature in II/R, intestinal morphological staining, and immunohistochemistry were performed. Histological evaluation by HE and Masson's trichrome staining revealed decreased microvessel histological damage and Chiu scores in *Pad4*-deficient mice that underwent II/R compared with those in WT II/R mice (Fig. 2H and I). Immunohistochemistry analysis revealed that II/R injury-induced increases in the number of TUNEL-positive cells, VCAM-1 upregulation, and plasma albumin leakage from vessels into the interstitial tissue. However, *Pad4* deficiency ameliorated cell apoptosis, decreased VCAM-1 expression, and weakened the diffusion of plasma albumin into the outer surface of the vessel wall (Fig. 2H and I). In addition, *Pad4* ablation stabilized syndecan-1 in the intestine and attenuated its loss and release into the serum after II/R injury (Fig. 2J). Finally, TEM was used to confirm morphological changes in intestinal microvascular endothelial cells. As shown in Fig. 2K, irregular endothelial swelling and luminal stenosis, accompanied by microthrombosis (indicated by the black arrow), were observed in intestinal microvessels following II/R injury in WT mice but not in neutrophil-specific *Pad4*-KO mice. These results indicated that NETs drove intestinal microvascular hyperpermeability and dysfunction, and the clearance of NETs (*Pad4* deficiency) in the II/R ileum may reduce intestinal microvessel injury.

3.3. NET formation promoted ferroptosis of intestinal vascular endothelial cells

To further explore how NETs lead to intestinal microvascular damage, HUVECs were cultured in the presence of isolated NETs (500 ng/mL) for 24 h, and RNA sequencing was performed on the total RNA extracted. PCA of Blank versus NET treatment revealed a clear separation between the two groups (Fig. 3A). Genes with a *P* value < 0.05 and $|\log_2 FC| > 1.5$ were considered to be differentially expressed. Based on these criteria, 2126 mRNAs were upregulated, and 4247 mRNAs were downregulated in HUVECs cultured with NETs, as shown in the bar graph (Fig. 3B) and volcano plot (Fig. 3C). Next, KEGG and GO pathway enrichment analyses of differentially expressed genes were performed,

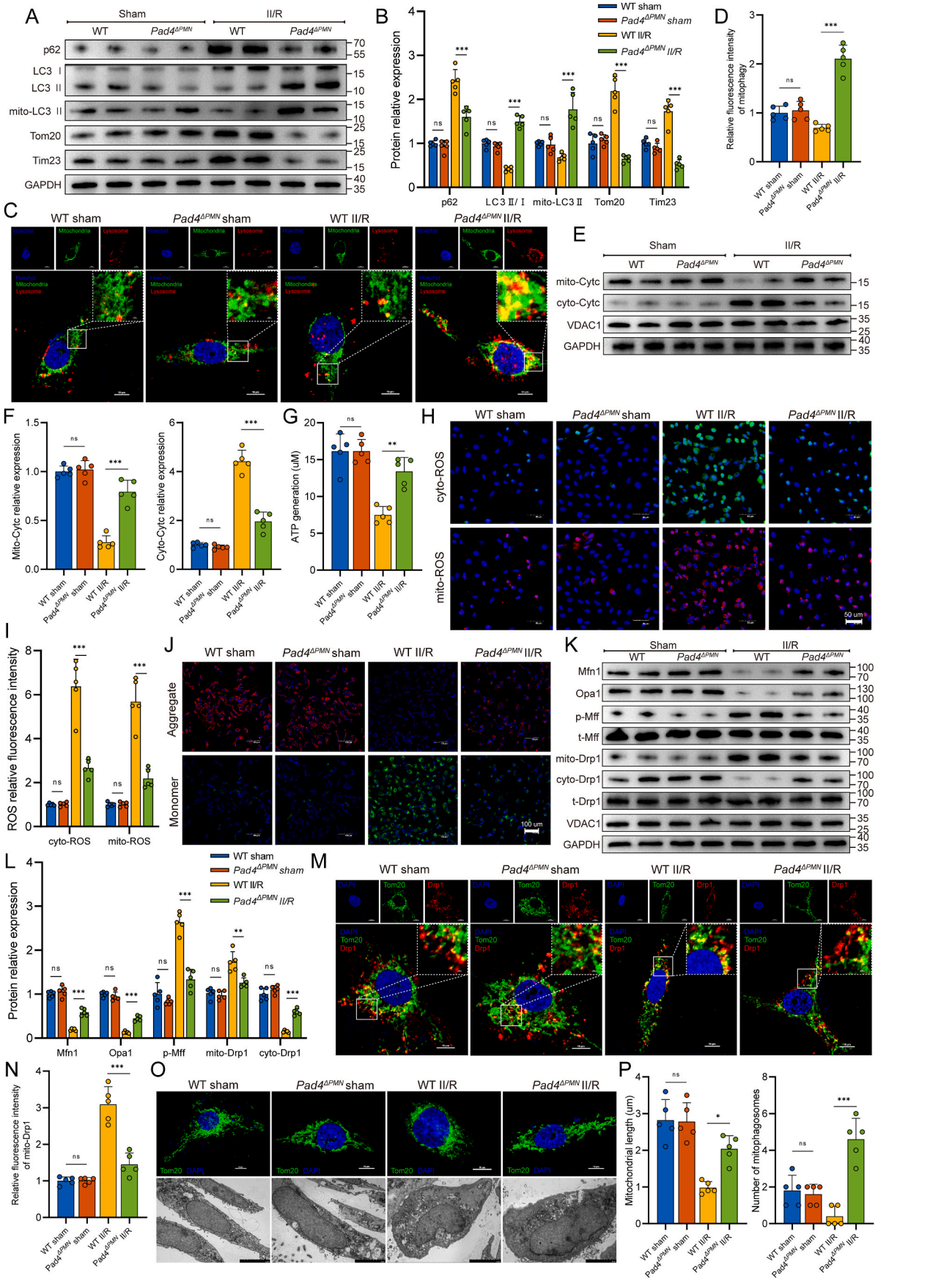

(caption on next page)

Fig. 5. NET formation negatively impacted mitochondrial quality control in the microvascular endothelium of the intestine. A-B. Western blotting to assess mitophagy flux (p62, LC3 II/I ratio and mito-LC3 II) and mitochondrial protein (Tom20 and Tim23) levels in the intestinal endothelium of WT and *Pad4*$^{\Delta PMN}$ mice. **C-D.** To evaluate the level of mitophagy, colocalization of mitochondria (MitoTracker) and lysosomes (LysoTracker) was analyzed using immunofluorescence. **E-F.** Western blotting was used to investigate the Cytc levels in both the cytosol and isolated mitochondria of intestinal endothelial cells. **G.** ATP generation was measured using an ATP assay kit. **H–I.** Cytoplasmic and mitochondrial ROS were measured using DCFH-DA and MitoSOX Red probes. **J.** The mitochondrial membrane potential of isolated intestinal endothelial cells was examined by JC-1 staining. **K-L.** Western blotting was used to analyze the regulatory factors related to mitochondrial fusion (Mfn1 and Opa1) and fission (Mff and Drp1). **M-N.** Immunofluorescence detection of mitochondrial fission was accomplished by costaining Drp1 and mitochondria. Drp1 exhibits a propensity to interact with fragmented mitochondria. **O–P.** Morphological alterations in mitochondria were observed using immunofluorescence (Tom20) and TEM. The average mitochondrial length and the numbers of mitophagosomes were determined. TEM, transmission electron microscopy. Data are expressed as the means ± SD, ns, not significant, $^{*}P < 0.05$, $^{**}P < 0.01$, $^{***}P < 0.001$.

and the top 20 most significantly enriched KEGG pathways (Fig. 3D) and GO terms (Fig. 3E–G) are listed. Moreover, we compared these differentially expressed genes with programmed cell death-related genes in the GO database (http://www.geneontology.org/) and found that 1112 genes were significantly differentially expressed (Fig. 3H). The number of differentially expressed genes associated with ferroptosis was the highest among all programmed cell death-related differential genes (Fig. 3I), including 22 upregulated and 64 downregulated genes (Fig. 3J). These data showed that endothelial cell ferroptosis might correlate with NET-induced microvascular damage.

To detect ferroptosis in intestinal microvessels of II/R patients, we isolated intestinal endothelial cells using magnetic bead cell sorting with a CD31 antibody. As shown in Fig. 3K, ELISA results revealed that MDA, GSSG, and Fe^{2+} levels were significantly increased in intestinal vascular endothelial cells of II/R patients, while GSH levels were markedly diminished. In addition, mRNA levels of *GPx4* in intestinal vascular endothelial cells of II/R patients were markedly decreased (Fig. 3L), which was accompanied by decreased GPx4 protein expression (Fig. 3M and N). In contrast, the mRNA and protein levels of ACSL4 were significantly elevated. These results indicate that II/R-induced intestinal microvascular injury is related to endothelial cell ferroptosis. Alternatively, NET formation may be involved in the activation of ferroptosis.

3.4. Targeted regulation of ferroptosis affects NET-mediated intestinal microvascular damage

To further define the molecular links among NET formation, intestinal vascular endothelial cell ferroptosis, and microvessel damage, we administered erastin (a ferroptosis activator) and ferrostatin-1 (a ferroptosis inhibitor) to target ferroptosis in WT and *Pad4*$^{\Delta PMN}$ II/R mice (Suppl. Fig. 1A). We first examined global NET formation in the intestine. As shown in Fig. 4A, the ferroptosis inhibitor and activator did not alter the levels of CitH3-DNA and MPO-DNA complexes in the intestine after II/R treatment. Furthermore, no differences were detected between the erastin and ferrostatin-1 groups in Ly6G or CitH3 expression (Fig. 4B and C). These results indicated that the regulation of ferroptosis by treatment with erastin or ferrostatin-1 did not affect neutrophil infiltration or NET formation in WT or *Pad4*$^{\Delta PMN}$ II/R mice.

Considering that cellular ferroptosis is a dynamic process, we analyzed the cell count and viability of isolated endothelial cells. Additionally, the changes over time in cell morphology and ferroptosis biomarkers were also documented. As shown in Suppl. Figs. 1B and C, the cell count and viability of intact endothelial cells isolated from the intestines in WT II/R mice were decreased compared to the WT sham group. While the morphological differences of isolated fresh endothelial cells (0 h) may not be evident under an optical microscope (Suppl. Fig. 1D), the cell activity of the WT II/R group is significantly diminished (Suppl. Fig. 1E). This alteration is associated with heightened ferroptosis levels and the accumulation of markers for endothelial injury, showing a positive correlation with the duration of incubation (Suppl. Figs. 1F and G). To minimize potential interference from other factors, we opted for freshly isolated endothelial cells (0 h) for further experimentation.

We further examined ferroptosis-related indicators in microvascular endothelial cells isolated from the intestine using CD31 magnetic beads. WT II/R mice showed significantly increased MDA, GSSH, and Fe^{2+} levels and decreased GSH levels compared to those in sham mice, while ferrostatin-1 markedly decreased MDA, GSSH, and Fe^{2+} levels and increased GSH production (Fig. 4D). Interestingly, similar effects were also observed in the *Pad4*$^{\Delta PMN}$ II/R group. *Pad4* deficiency notably reduced MDA, GSSG, and Fe^{2+} levels and elevated the GSH content compared to those in WT II/R mice. However, these effects could be reversed by the ferroptosis activator erastin. In addition, WB analyses showed that GPx4 and FTH1 were downregulated in the WT II/R mice, while the ACSL4 and COX2 levels were upregulated (Fig. 4E and F). In contrast, *Pad4* deficiency suppressed COX2 and ACSL4 expression and restored GPx4 and FTH1 levels. Overall, these results confirmed the upstream and downstream relationships between NET formation and intestinal microvascular endothelial cell ferroptosis, and the regulation of NET formation could affect ferroptosis in the microvessel endothelium.

We next examined the relationship between endothelial cell ferroptosis and intestinal microvascular injury. As shown in Fig. 4G and H, ferrostatin-1 significantly attenuated the impaired intestinal blood perfusion in WT II/R mice. However, erastin reversed the protective effect of blood flow perfusion afforded by *Pad4* deficiency during II/R. Histopathological staining and immunohistochemistry showed that the application of ferrostatin-1 alleviated pathological injury to the intestinal microvasculature, decreased the number of apoptotic cells, diminished VCAM-1 expression, and ameliorated plasma albumin exudation in the WT II/R group (Suppl. Figs. 2A and B). The same trends were observed in *Pad4*-deficient mice, while these protective effects were reversed by the administration of erastin (Suppl. Figs. 2A and B). Furthermore, immunofluorescence revealed upregulated CitH3 infiltration around intestinal microvessels in both the WT II/R group and the ferrostatin-1- or erastin-treated group (Fig. 4I). Notably, although there was little appreciable reduction in NET formation, elevated VE-cadherin expression was observed in the ferrostatin-1-treated WT II/R group. Although no significant intestinal NET formation was observed in the *Pad4*-deficient II/R group, with or without ferrostatin-1 or erastin treatment, erastin reversed the preserving effect of *Pad4* ablation on VE-cadherin. Similar WB results verified this observation at the protein level (Fig. 4J and K). These results further defined the upstream or downstream relationships among NET formation, endothelial cell ferroptosis, and microvascular dysfunction. NETs may lead to microvascular injury through the regulation of intestinal endothelial ferroptosis.

3.5. Elevated NET formation impaired mitochondrial quality control in intestinal vascular endothelial cells

The KEGG pathway analysis also showed enrichments of mitophagy- and lysosome-associated pathways (Fig. 3D). Considering that mitochondrial dysfunction is closely related to ferroptosis, we further assessed whether mitochondrial function in intestinal microvascular endothelial cells was affected by NET formation. Intestinal endothelial cells were isolated and collected from WT and *Pad4*$^{\Delta PMN}$ mice using CD31 magnetic beads. Subsequently, western blotting detected mitophagy-associated proteins (Fig. 5A and B). The results demonstrated a significant increase in SQSTM1/p62 expression and decreases in the LC3 II/I ratio and mito-LC3 II expression. Conversely, *Pad4* deficiency diminished SQSTM1/p62 expression and restored mito-LC3 II

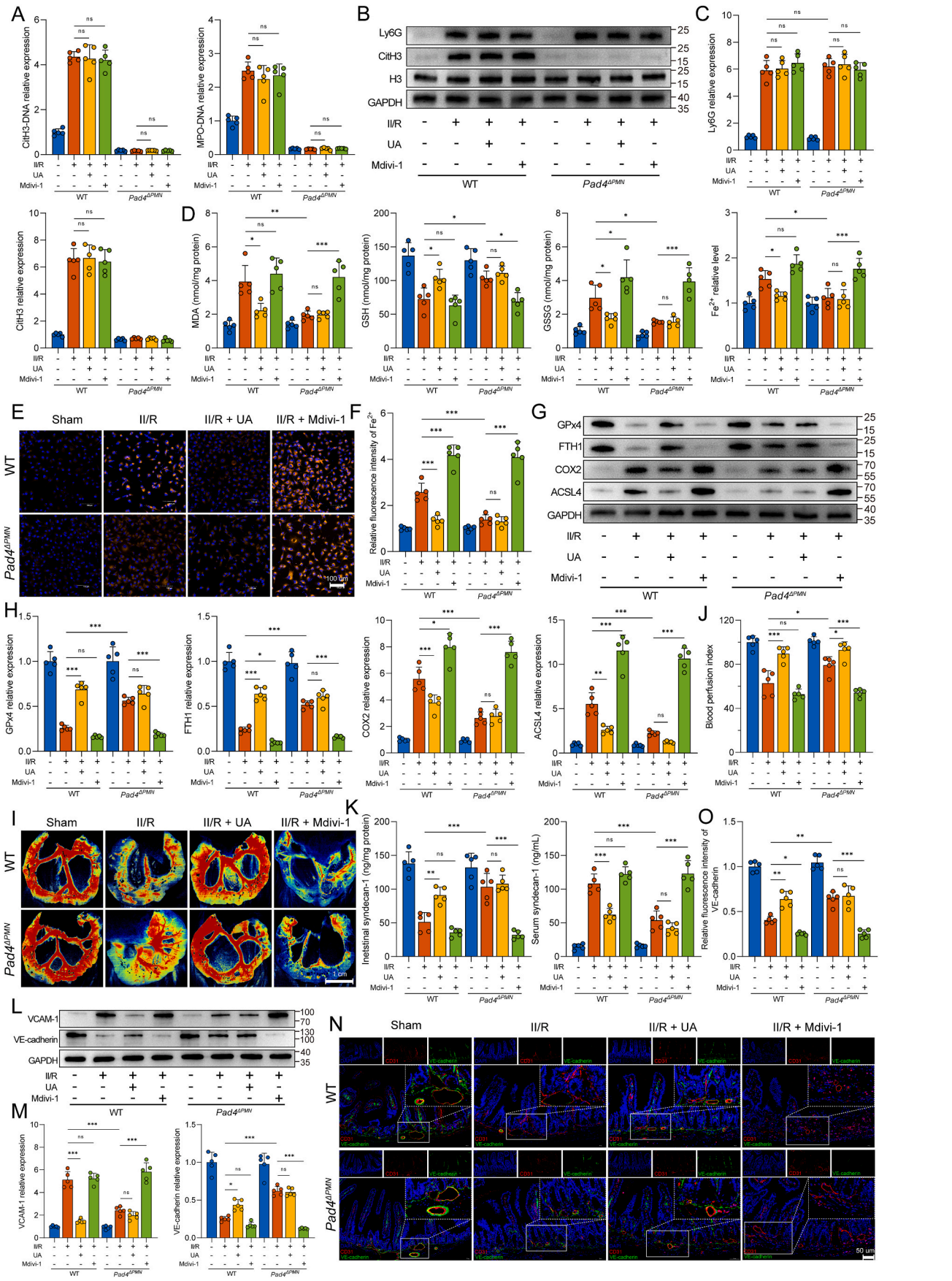

(caption on next page)

Fig. 6. Mitophagy regulation impacts NET-induced intestinal microvascular endothelial cell ferroptosis and dysfunction. A. CitH3-DNA and MPO-DNA complexes in the intestine were assessed using ELISAs. **B–C**. Western blotting was performed to detect relevant proteins of neutrophil infiltration (Ly6G) and NET formation (CitH3) in the intestine. **D**. Isolated endothelial cells from intestinal tissue were used to assess intracellular MDA, GSH, GSSH and Fe^{2+} levels by ELISAs. **E-F**. Fluorometric analysis of intracellular Fe^{2+} using FerroOrange. **G-H**. Levels of ferroptosis-related proteins in the intestinal microvascular endothelium were determined by western blotting. **I-J**. Laser speckle imaging was used to assess intestinal blood perfusion. **K**. Syndecan-1 concentrations in the serum and intestinal homogenate were determined using ELISA kits. **L-M**. Quantification of the intestinal microvascular damage markers VCAM-1 and VE-cadherin was performed by Western blot analysis. Grayscale images were analyzed using the ImageJ software. **N–O**. Immunofluorescence colocalization of a microvascular biomarker (CD31) and VE-cadherin in the intestine was performed to assess microvascular damage. Scale bars = 50 μm. Data are presented as the means ± SD, ns, not significant, $^{*}P < 0.05$, $^{**}P < 0.01$, $^{***}P < 0.001$.

expression, with concomitant decreases in mitochondrial Tom20 and Tim23 levels. Additionally, less colocalization of mitochondria and lysosomes was observed in intestinal endothelial cells in the WT II/R group by costaining with LysoTracker Red and MitoTracker Green (Fig. 5C and D). In contrast, *Pad4* deficiency increased the colocalization of mitochondria and lysosomes, suggesting that mitophagosome formation was significantly augmented following NET inhibition. Subsequently, changes in intestinal endothelial mitochondrial function were assessed. As shown in Fig. 5E and F, there was a significant accumulation of the cytosolic Cytc protein in WT II/R mice and a remarkable moderation of this effect in *Pad4*-deficient mice. Moreover, mice treated with II/R showed significantly decreased ATP generation (Fig. 5G), elevated cyto- and mito-ROS production (Fig. 5H and I), and a lowered $\Delta\Psi$m level (Fig. 5J). However, ATP generation was increased, cyto- and mito-ROS overproduction was alleviated, and $\Delta\Psi$m was stabilized in $Pad4^{\Delta PMN}$ mice.

Subsequently, we examined the effect of NET formation on mitochondrial fusion and fission in intestinal vascular endothelial cells. As shown in Fig. 5K and L, fusion-related proteins, such as Mfn1 and Opa1, were downregulated after II/R treatment, but this reduction was ameliorated in *Pad4*-deficient mice. Western blotting also examined the molecular mechanism underlying II/R-related mitochondrial fission. The results revealed that Mff phosphorylation was markedly increased in response to II/R treatment. II/R promoted Drp1 translocation from the cytosol to mitochondria, which initiated mitochondrial fission. In contrast, the *Pad4* deletion mitigated Mff phosphorylation and reduced the level of mitochondrial Drp1 (Fig. 5K and L). Colocalization of mitochondria and Drp1 puncta by immunofluorescence showed that II/R injury increased the number of Drp1-labeled fragmented mitochondria. However, *Pad4* deficiency led to the preservation of the mitochondrial network and restrained the translocation of Drp1 to mitochondria (Fig. 5M and N). In addition, morphological changes in mitochondria were observed by immunofluorescence and TEM. II/R induced mitochondrial fragmentation, accompanied by mitochondrial swelling and vacuolization, outer membrane rupture, cristae disappearance, and mitophagosome loss. However, the *Pad4* ablation resulted in predominantly elongated forms of mitochondria and promoted mitophagosome formation (Fig. 5O and P). Therefore, these results confirmed our hypothesis that NET formation impaired intestinal endothelial mitochondrial quality control and augmented mitochondrial dysfunction in the II/R injury setting.

3.6. Modulation of mitophagy impacts NET-induced intestinal microvascular endothelial ferroptosis and dysfunction

Our results suggested that NET formation could suppress mitophagy in intestinal microvascular endothelial cells; however, the current context's relationship between mitophagy and ferroptosis remained unclear. We next used UA (urolithin A, a mild mitophagy activator) and Mdivi-1 (mitochondrial division inhibitor 1, a mitophagy inhibitor) to examine the association between mitophagy and ferroptosis in both WT and $Pad4^{\Delta PMN}$ mice (Suppl. Fig. 3A). We first examined NET formation in the intestine. The results showed that the current UA or Mdivi-1 administration mode did not influence intestinal NET levels (Fig. 6A–C). Next, intestinal endothelial cells were isolated using magnetic bead cell sorting with a CD31 antibody to assess ferroptosis. As shown in Fig. 6D, the MDA, GSSG, and Fe^{2+} levels were significantly increased due to II/R injury but significantly decreased by UA administration in WT mice. However, the mitophagy inhibitor Mdivi-1 reversed the *Pad4* deficiency-mediated inhibition of MDA, GSSG, and Fe^{2+} levels and the sustention of GSH levels. The same trend was shown for Fe^{2+} staining with FerroOrange (Fig. 6E and F). We next assessed the expression levels of ferroptotic proteins using western blotting. Treatment with the mitophagy activator UA increased the relative expression of FTH1 and GPx4 and reduced that of ACSL4 and COX2 in WT II/R mice. In contrast, FTH1 and GPx4 were downregulated, while ACSL4 and COX2 were upregulated in the WT and $Pad4^{\Delta PMN}$ mice administered Mdivi-1 (Fig. 6G and H). These results revealed that mitophagy regulation was associated with ferroptosis levels. Notably, no visible changes in mitophagy-related protein levels in response to erastin or ferrostatin-1 were observed in intestinal microvascular endothelial cells from WT or *Pad4*-deficient mice (Suppl. Figs. 3B and C). Altogether, these results confirmed the regulatory relationship between mitophagy and ferroptosis.

We further evaluated the effect of mitophagy regulation on intestinal microvessel function. As shown in Fig. 6I and J, UA enhanced intestinal blood perfusion in both WT and $Pad4^{\Delta PMN}$ II/R mice, while the mitophagy inhibitor Mdivi-1 reversed this effect. The results of histopathological staining and immunohistochemistry demonstrated that the administration of UA mitigated pathological damage to the intestinal microvasculature, diminished the Chiu score, reduced the quantity of apoptotic cells, attenuated the elevated expression of VCAM-1, and weakened plasma albumin leakage in the WT II/R group. However, these protective effects were reversed by Mdivi-1 application in both the WT and *Pad4*-deficient II/R groups (Suppl. Figs. 3D and E). Furthermore, UA demonstrated the ability to stabilize the glycoprotein syndecan-1 in endothelial cells and mitigate its migration to the serum after II/R injury. Conversely, Mdivi-1 elicited a greater release of syndecan-1 into circulation (Fig. 6K). Moreover, intestinal VCAM-1 and VE-cadherin protein expression was measured by western blotting to evaluate microvascular damage. UA administration reduced VCAM-1 expression while simultaneously increasing VE-cadherin expression in the WT II/R group. However, the Mdivi-1 treatment reversed these effects in the WT and *Pad4*-deficient groups (Fig. 6L and M). Additionally, the immunofluorescence results confirmed these observations regarding the VE-cadherin expression levels (Fig. 6N and O). The data suggest that NETs may induce ferroptosis by suppressing mitophagy levels. Selective activation of mitophagy may mitigate NET-induced ferroptosis and dysfunction of intestinal endothelial cells.

3.7. Fundc1-mediated mitophagy is required for attenuating ferroptosis and maintaining microvascular function

Mitophagy is a complex metabolic process regulated by several upstream signaling pathways. Given that ischemia or hypoxic stimuli primarily impact Fundc1 phosphorylation, our study sought to examine the potential involvement of the Fundc1 signaling pathway in NET-mediated mitophagy regulation. As shown in Suppl. Figs. 4A and B, II/R augmented Fundc1 phosphorylation at Tyr18 and diminished Ser17 phosphorylation in intestinal endothelial cells, while these responses in *Pad4*-deficient mice were partially reversed. Furthermore, we used an adeno-associated virus carrying a *Fundc1* shRNA under the control of the

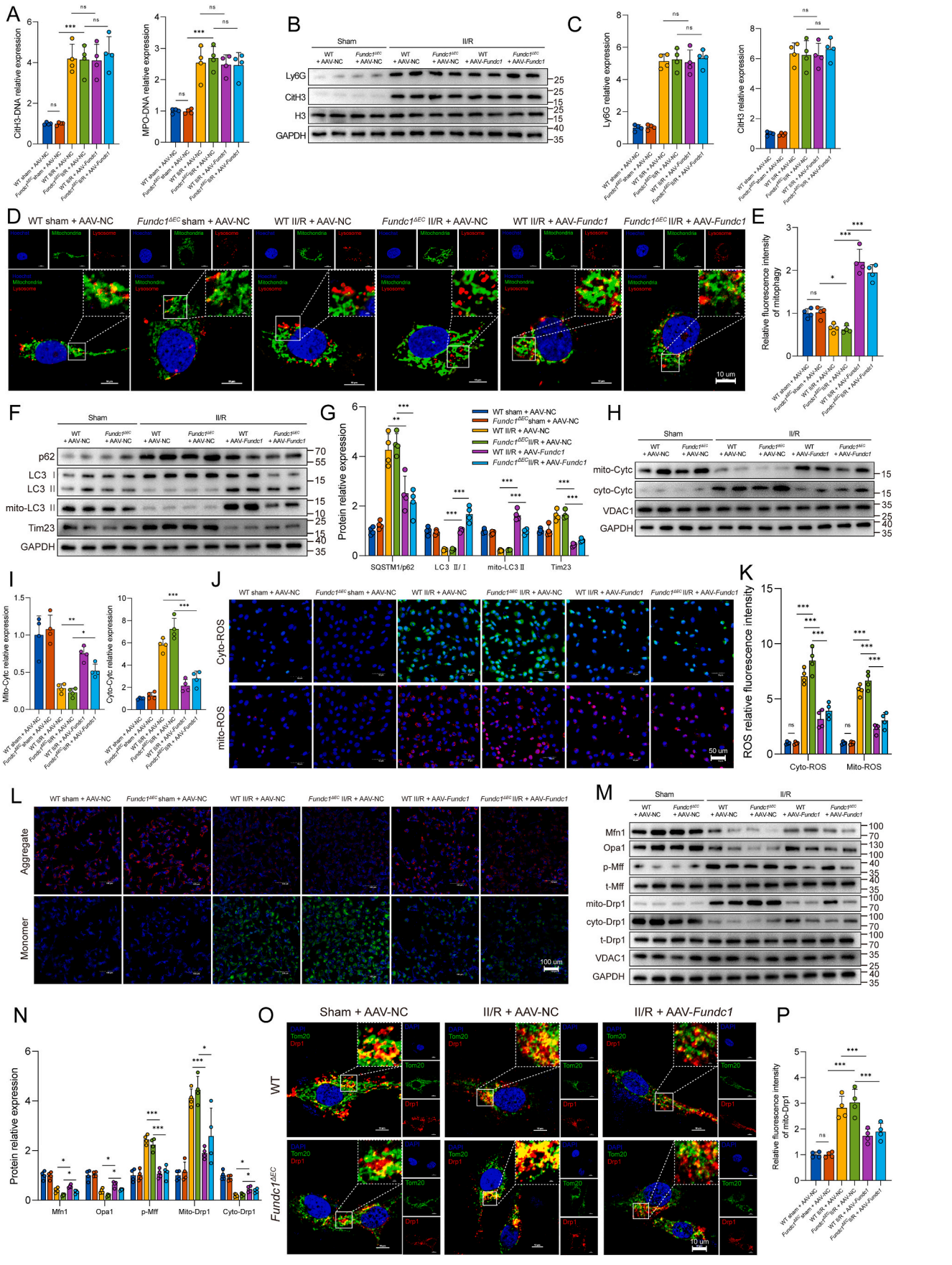

(caption on next page)

Fig. 7. Effects of Fundc1 regulation on NET formation and endothelial mitochondrial quality control. A. Intestinal CitH3-DNA and MPO-DNA complexes were assayed using ELISAs. **B–C**. Protein expression levels of Ly6G and CitH3 were measured by Western blot analysis. **D-E**. Intestinal CD31-positive endothelial cells were isolated with CD31-coated magnetic beads. Mitochondrial (MitoTracker) and lysosomal (LysoTracker) immunofluorescence colocalization was performed to explore the mitophagy level. **F-G**. Endothelial mitophagy parameters (p62, LC3 II/I ratio and mito-LC3 II) and a mitochondrial protein (Tim23) were examined using western blotting. The relative grayscale values were measured using ImageJ. **H–I**. Cytc levels in the cytosol and isolated mitochondria were examined by western blotting. **J-K**. Quantification of cytoplasmic and mitochondrial ROS in the intestinal endothelium was conducted using DCFH-DA and MitoSOX Red probes. **L**. Mitochondrial membrane potential changes in endothelial cells were detected by JC-1 staining. **M-N**. Key proteins of mitochondrial fusion (Mfn1 and Opa1) and fission (Mff and Drp1) were examined by a Western blot assay. **O–P**. Immunofluorescence confocal imaging of mitochondrial (Tom20, green) and Drp1 (red) colocalization was used to evaluate mitochondrial fission. AAV, adeno-associated virus; NC, negative control. Data are shown as the means ± SD, ns, not significant, $^{*}P < 0.05$, $^{**}P < 0.01$, $^{***}P < 0.001$.

TIE1 promoter to specifically knock down Fundc1 expression in the endothelium. Endothelium-specific Fundc1 knockdown reversed the reduction in MDA, GSSG, and Fe^{2+} levels and decreased GSH levels in intestinal microvascular endothelial cells of *Pad4*-deficient II/R mice (Suppl. Fig. 4C). Moreover, the knockdown of *Fundc1* resulted in increased ferroptosis in $Pad4^{\Delta PMN}$ II/R mice, which was manifested as decreased expression of the GPx4 and FTH1 proteins and increased expression of the COX2 and ACSL4 proteins (Suppl. Figs. 4D and E). In addition, the WB results revealed that VCAM-1 level increased and VE-cadherin levels decreased in the intestine after AAV-sh*Fundc1* treatment of *Pad4*-deficient mice (Suppl. Figs. 4F and G), indicating that Fundc1 knockdown abolished the protective effect of *Pad4* deficiency on intestinal microvascular function. These results indicated that the Fundc1 protein might be a key regulator of NET-induced mitophagy suppression.

To further explore whether Fundc1-mediated mitophagy is involved in ferroptosis and microvascular dysfunction, an endothelial cell-specific inducible Fundc1 knockout mouse line ($Fundc1^{\Delta EC}$) and AAV9 carrying *Fundc1* under control of the TIE1 promoter were used in the following experiments (Suppl. Fig. 4H). Initially, the formation of intestinal NETs was investigated. The findings indicated that *Fundc1* deficiency, with or without supplementation with exogenous Fundc1 (AAV-*Fundc1*), did not elicit any discernible impact on the levels of NETs in the intestinal region following II/R injury (Fig. 7A–C). Subsequently, costaining with LysoTracker Red and MitoTracker Green demonstrated less colocalization of mitochondria and lysosomes in intestinal endothelial cells in the *Fundc1*-deficient group. Fundc1 supplementation via AAV-*Fundc1* increased mitophagosome numbers in both WT and *Fundc1*-deficient II/R mice (Fig. 7D and E). Meanwhile, western blotting detected mitophagy-associated proteins (Fig. 7F and G). The findings revealed a noteworthy elevation in SQSTM1/p62 and Tim23 expression and reduced the LC3 II/I ratio and mito-LC3 II expression in the *Fundc1*-deficient II/R group. In contrast, intraperitoneal injection of AAV-*Fundc1* partially led to a decline in SQSTM1/p62 and Tim23 expression and a resurgence of the LC3 II/I ratio and mito-LC3 II expression in both the WT and $Fundc1^{\Delta EC}$ groups following II/R injury. Next, an evaluation of changes in intestinal endothelium mitochondrial function was conducted. II/R plus AAV-NC treatment of $Fundc1^{\Delta EC}$ mice resulted in a significant augmentation in the release of Cytc from mitochondria into the cytosol (Fig. 7H and I), an elevation in cyto- and mito-ROS generation (Fig. 7J and K), and a decrease in the $\Delta\Psi m$ level (Fig. 7L). Meanwhile, pretreatment with AAV-*Fundc1* partially reversed these changes. Next, we investigated the fusion and fission of mitochondrial structures in intestinal vascular endothelial cells. Our findings, as illustrated in Fig. 7M and N, indicated a decrease in the expression of fusion-related proteins, such as Mfn1 and Opa1, following II/R treatment of $Fundc1^{\Delta EC}$ mice. However, this reduction was mitigated in WT and *Fundc1*-deficient mice pretreated with AAV-*Fundc1*. The results also demonstrated a significant increase in Mff phosphorylation in response to II/R treatment (Fig. 7M and N), as well as the promotion of Drp1 translocation from the cytosol to mitochondria (Fig. 7M–P) in WT and $Fundc1^{\Delta EC}$ II/R mice. However, AAV-*Fundc1* pretreatment resulted in the retention of the mitochondrial network and inhibited the migration of Drp1 to mitochondria. This suggests that Fundc1 is vital in maintaining mitochondrial quality control in the intestinal endothelium.

We further examined the effects of Fundc1 regulation on endothelial cell ferroptosis and microvascular function in the intestine. Fig. 8A demonstrates that II/R injury led to significant increases in MDA, GSSG, and Fe^{2+} levels and a decrease in GSH levels in $Fundc1^{\Delta EC}$ mice, which were subsequently reversed by AAV-*Fundc1* administration in WT and *Fundc1*-deficient mice. The trend of changes in the Fe^{2+} levels was further confirmed by FerroOrange staining (Fig. 8B and C). WB analysis revealed relative increases in ACSL4 and COX2 expression and decreases in FTH1 and GPx4 expression in WT and $Fundc1^{\Delta EC}$ II/R mice (Fig. 8D and E). Moreover, *Fundc1* deficiency blocked intestinal blood perfusion following II/R, while pretreatment with AAV-*Fundc1* partially restored the blood perfusion index (Fig. 8F and G). AAV-*Fundc1* transfection could stabilize the syndecan-1 glycoprotein in endothelial cells and hinder its migration to the serum following II/R injury in the WT and $Fundc1^{\Delta EC}$ II/R groups (Fig. 8H). Meanwhile, the findings from histopathological staining and immunohistochemistry demonstrated that AAV-*Fundc1* administration attenuated the pathological injury to intestinal microvessels, reduced the Chiu score, decreased the number of TUNEL-positive cells, mitigated VCAM-1 expression, and restrained plasma albumin leakage in WT and $Fundc1^{\Delta EC}$ mice after II/R injury (Fig. 8I and J). Furthermore, western blotting was used to assess microvascular injury by measuring intestinal VCAM-1 and VE-cadherin protein expression (Fig. 8K and L). The WT and $Fundc1^{\Delta EC}$ II/R groups exhibited decreased VE-cadherin expression and a concomitant increase in VCAM-1 expression. However, AAV-*Fundc1* treatment counteracted these effects in the WT and *Fundc1*-deficient groups. The immunofluorescence results further corroborated these findings, which demonstrated a similar trend in the intestinal VE-cadherin expression level (Fig. 8M and N). These results indicated that NETs might impair intestinal microvascular endothelial mitophagy via the Fundc1 protein. Deletion of Fundc1 resulted in mitochondrial quality control failure, ferroptosis aggravation, and microvascular damage.

4. Discussion

The topic of intestinal microvascular ischemia–reperfusion injury has been overlooked in perioperative gut barrier protection. Owing to the intricate molecular mechanisms underlying II/R-induced microvascular dysfunction, limited pharmacological options are available for safeguarding intestinal microcirculation against such injury. In this study, we first established heightened NET formation, intestinal endothelial cell ferroptosis activation, and microvascular dysfunction in intestinal samples obtained from II/R patients. Moreover, it was observed that the inhibition of NET formation through neutrophil-specific *Pad4* deficiency led to the mitigation of intestinal endothelial ferroptosis and microvascular dysfunction induced by II/R in vivo. These findings support the notion that NETs play a detrimental role in intestinal vascular barrier damage under II/R conditions. Furthermore, the study revealed a novel finding, indicating that NETs can initiate endothelial ferroptosis by impeding the activation of Fundc1-requiring mitophagy (Fig. 9).

II/R injury is an important factor associated with high mortality and prolonged hospitalization [22,44]. The intestine, a crucial organ endowed with a profuse vascular network, is highly susceptible to ischemia and reperfusion injury [45]. The occurrence of I/R in intestinal

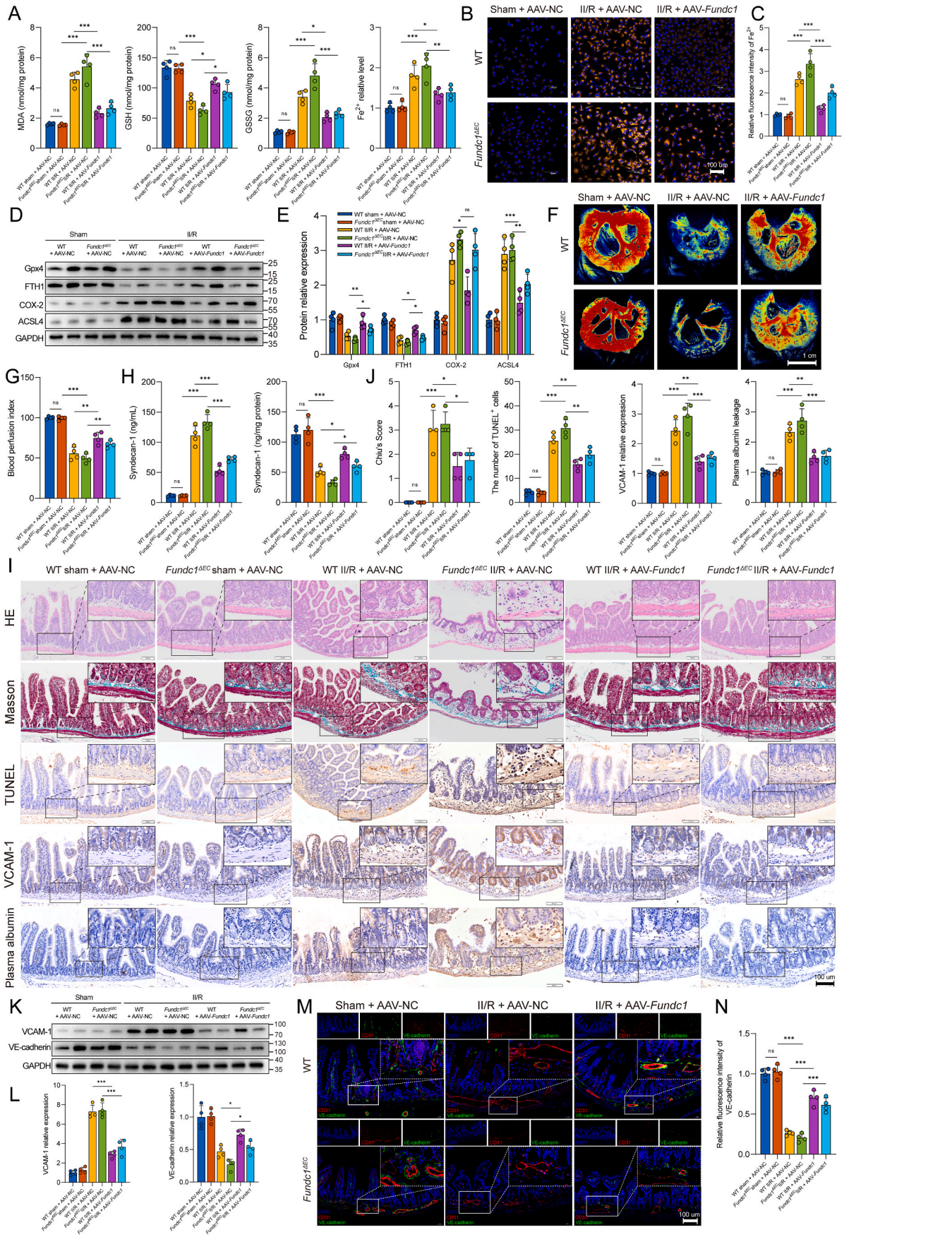

(caption on next page)

Fig. 8. Impact of Fundc1 regulation on the intestinal endothelial ferroptosis level and microvascular function. A. Endothelial cells isolated from intestinal tissue were used to evaluate MDA, GSH, GSSH and Fe^{2+} levels by ELISAs. **B–C**. Intracellular Fe^{2+} in the intestinal endothelium was evaluated using the FerroOrange probe. **D-E**. Western blot analysis was used to detect ferroptosis-related proteins in endothelial cells isolated from the intestine. **F-G**. Intestinal blood perfusion in WT and *Fundc1*$^{\Delta EC}$ mice was measured using a laser speckle blood flow analysis system. **H**. Intestinal and serum syndecan-1 levels were assessed using an ELISA kit. **I-J**. Pathological staining and immunohistochemistry were performed to evaluate intestinal microvascular function. The intestinal microvascular morphology was observed by HE and Masson's trichrome staining and evaluated and graded according to the Chiu score system. TUNEL staining was used to evaluate microvascular cells undergoing apoptosis. Intestinal microvascular damage and permeability were assessed using immunohistochemistry for VCAM-1 and albumin. **K-L**. Western immunoblotting was used to examine VCAM-1 and VE-cadherin protein expression. **M-N**. To evaluate microvascular damage, immunofluorescence colocalization of CD31 and VE-cadherin was conducted in the intestine. Data correspond to the means ± SD, ns, not significant, $^{*}P < 0.05$, $^{**}P < 0.01$, $^{***}P < 0.001$.

tissues can stimulate the release of reactive oxygen species and associated inflammatory mediators, instigating the aggregation and activation of neutrophils within the intestine [46]. The persistence of activated neutrophils could exacerbate local intestinal damage, culminating in the impairment of the gut barrier and translocation of intestinal bacteria and endotoxins [47,48]. Our prior research on rats revealed that II/R injury could result in intestinal inflammation and a reduction in the levels of tight junction proteins [16]. The intestinal barrier comprises the intestinal epithelial barrier, consisting of intestinal epithelial cells, and the intestinal vascular barrier, consisting of vascular endothelial cells, enteric glial cells, and pericytes [49,50]. While studies on the intestinal barrier have primarily focused on the epithelial barrier, there remains a dearth of understanding regarding the functions and molecular underpinnings of vascular barrier dysfunction in the context of II/R injury. Recent research has demonstrated that ischemia–reperfusion induces endothelial cell swelling, subendothelial collagen exposure, leukocyte adhesion, and microthrombus formation, ultimately resulting in microvascular dysfunction [51,52]. Our current investigation similarly demonstrated heightened neutrophil infiltration, elevated microvascular damage, and hyperpermeability in human II/R patients. Additionally, animal studies have revealed evidence of microvessel damage and dysfunction, characterized by intensified neutrophil aggregation, increased microvascular permeability, and upregulation of biomarkers of endothelial injury. Moreover, we employed CD31-positive magnetic beads to isolate endothelial cells from the intestine to investigate the effects of II/R on endothelial cells. Throughout this procedure, dead cells or cell fragments that could not be captured by the magnetic beads were eliminated through centrifugation. As a result, the WT II/R group displayed a diminished count of endothelial cells compared to the sham group. Furthermore, despite the absence of discernible morphological disparities in the initially isolated intact endothelial cells when observed under an optical microscope, the WT II/R group exhibited a noteworthy decline in endothelial cell viability, accompanied by the accumulation of endothelial injury biomarkers. These results indicated that an increase in endothelial cell damage during II/R injury.

Activated neutrophils play a crucial role in eliminating pathogens through the release of NETs [7]. Nevertheless, overproduction of NETs may lead to local tissue damage, and NETs may act as a proinflammatory agent [8]. Our previous research has demonstrated that circulating NET biomarkers are linked to disease severity and clinical prognosis [15,53]. In the current study, we observed similar findings, as both MPO-DNA and CitH3-DNA complexes, which serve as intestinal NET biomarkers, were found to be elevated in serum and intestinal samples obtained from patients experiencing II/R injury. Furthermore, a positive correlation was observed between NET levels and microvascular injury biomarkers (syndecan-1 and vWF). Additionally, the presence of massive neutrophilic infiltration and NET formation in the intestinal microvasculature of II/R patients suggests a potential role for NET formation in endothelial injury. Notably, PAD4 is critical in regulating NET formation by facilitating histone decondensation through citrullination. To investigate the contribution of NETs to microvascular injury in the intestine during II/R, we conducted further investigations using mice with neutrophil-specific *Pad4* deficiency, which impedes NET formation. Our findings in an II/R animal model revealed that *Pad4* deficiency-mediated NET inhibition reduced NET formation around the microvascular lumen, resulting in improved microvessel permeability, enhanced microcirculatory perfusion, and alleviated pathological damage. Together, these results provide evidence of the deleterious effects of NETs in II/R-induced intestinal microvascular dysfunction.

Mitophagy is a crucial process that facilitates the removal of damaged and senescent mitochondria, thereby preserving mitochondrial homeostasis and cell viability [18,54]. Under physiological conditions, mitophagy and mitochondrial fusion, and fission work in tandem to maintain a balance in mitochondrial quality control and ensure optimal mitochondrial function [18,55]. However, when mitophagy is inhibited, the timely removal of impaired mitochondria is impeded, accumulating damaged mitochondria and subsequent mitochondrial dysfunction [27]. Evidence suggests that ischemia–reperfusion-induced tissue damage is intricately linked to mitochondrial dysfunction, governed by a complex regulatory mechanism [17,56,57]. Nevertheless, it remains unclear whether NETs play a role in mitochondrial dysfunction by impeding mitophagy, causing microvascular endothelial damage during II/R. The in vivo experimental findings from the present study demonstrated that NET formation hindered mitophagy levels and exacerbated mitochondrial dysfunction, resulting in a loss of mitochondrial membrane potential, overproduction of mt- and cyto-ROS, decreased mitochondrial ATP synthesis, elevated Cytc leakage, augmented mitochondrial fission and diminished mitochondrial fusion. However, the inhibition of mitophagy was significantly rescued, mitochondrial dysfunction was alleviated, and mitochondrial quality control was improved by *Pad4* deficiency or the mitophagy activator UA. Conversely, the use of the mitophagy inhibitor Mdivi-1 reversed the protective effects on the microvasculature and exacerbated mitochondrial dysfunction. These results provide compelling evidence that excessive NET formation hinders mitophagy, thereby exacerbating mitochondrial dysfunction.

The Fundc1 protein, which is located in the mitochondrial outer membrane and is highly conserved, functions as a mitophagy receptor that operates independently of ubiquitin and regulates both mitochondrial dynamics and mitophagy [20,58]. The activation of Fundc1-mediated mitophagy is preferentially induced by hypoxia and ischemia [59]. Fundc1 phosphorylation at Ser17 and Tyr18 results in different effects, as phosphorylation of Tyr18 inhibits Fundc1-mediated mitophagy, whereas phosphorylation of Ser17 enhances the interaction between mitochondria and LC3, thereby promoting mitophagy [19,60]. In the current investigation, we assessed the protein expression levels of p^{Ser17}-Fundc1, p^{Tyr18}-Fundc1, and t-Fundc1 in WT mice subjected to II/R and observed varying degrees of expression. However, in *Pad4*-deficient mice, we noted a significant decrease in p^{Tyr18}-Fundc1 expression and an increase in p^{Ser17}-Fundc1 expression. Consequently, we hypothesize that the coordinated action of these proteins ultimately leads to the suppression of mitophagy in WT II/R mice. Furthermore, we found that *Pad4* deficiency inhibited NET formation, which accounted for the dephosphorylation of Fundc1 at Tyr18 and the phosphorylation of Fundc1 at Ser17, ultimately resulting in the upregulation of mitophagy. To validate the hypothesis, endothelium-specific *Fundc1* knockout mice and an adeno-associated virus with specific expression of *Fundc1* in endothelial cells were employed to evaluate the impact of Fundc1-dependent mitophagy on intestinal microvascular dysfunction after II/R. *Fundc1* deficiency was found to reduce mitophagy levels, aggravate mitochondrial dysfunction, decrease mitochondrial fusion,

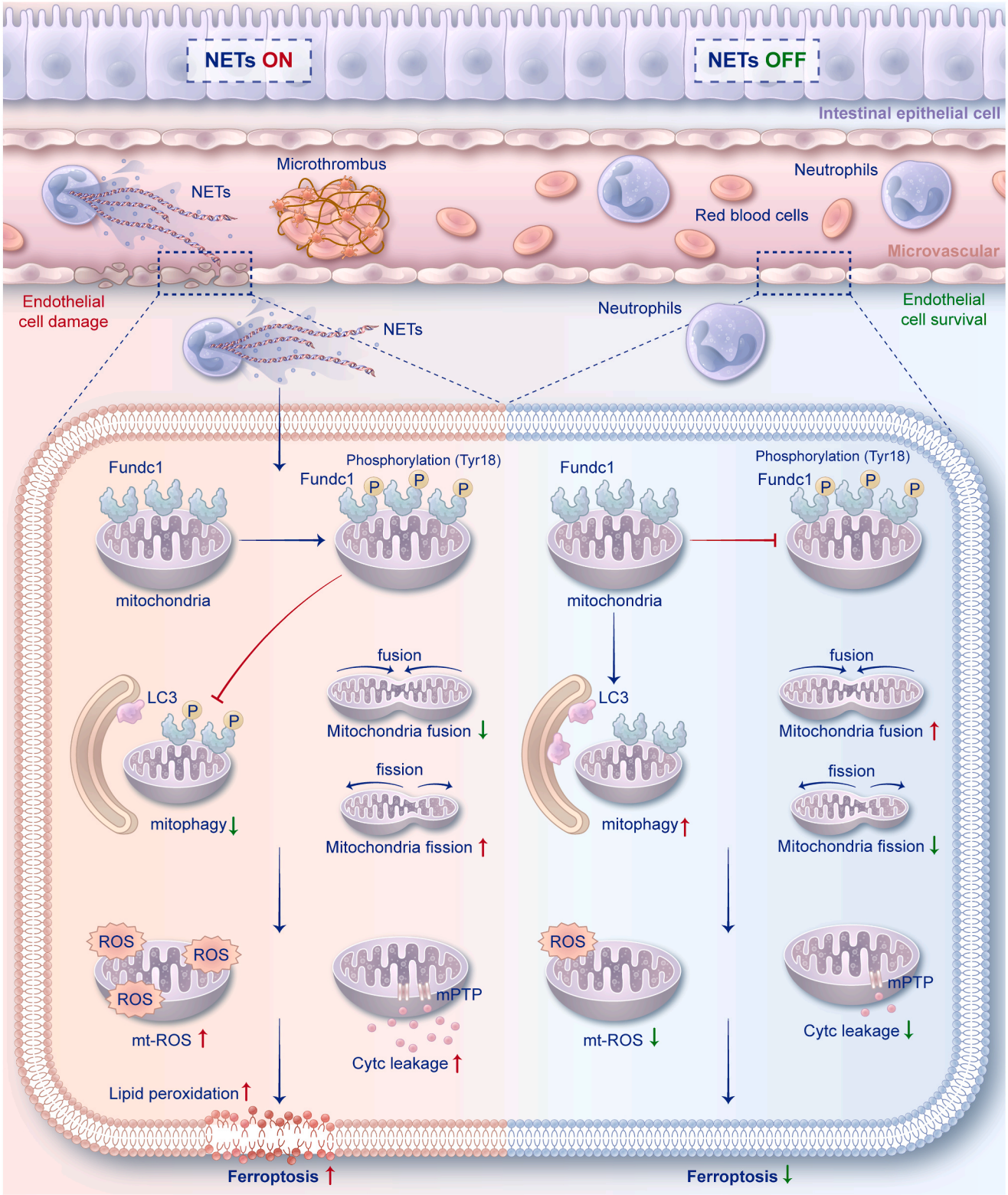

Fig. 9. During intestinal ischemia–reperfusion, neutrophils become activated and infiltrate the intestinal microcirculation by releasing NETs. The presence of NETs in microvessels affects endothelial cells, resulting in the phosphorylation of Fundc1 at Tyr18, which inhibits mitophagy function. Consequently, damaged mitochondria are not cleared promptly, leading to mitochondrial dysfunction, which is characterized by the accumulation of mitochondrial ROS and by Cytc leakage. The accumulation of intracellular and mitochondrial ROS triggers lipid peroxidation, which activates ferroptosis in endothelial cells, ultimately causing microvascular damage and dysfunction. The clearance of NETs has been shown to effectively maintain mitophagy levels in endothelial cells, leading to enhanced mitochondrial quality control and a reduction in mitochondrial dysfunction. As a result, ROS generation is mitigated, cell ferroptosis is prevented, and intestinal microvascular function is preserved.

increase mitochondrial fission, and intensify the disruption of the intestinal vascular barrier. However, the administration of AAV-*Fundc1* before II/R to WT and *Fundc1*-deficient mice partially reversed the aforementioned outcomes. Our data show that Fundc1-requiring mitophagy may play a pivotal role in NET-induced intestinal microvascular dysfunction.

Ferroptosis is a form of programmed cell death initiated by iron-dependent phospholipid peroxidation [23,61]. Recent research has revealed that ferroptosis is heightened during ischemia–reperfusion and that intervening in ferroptosis can mitigate damage to both the intestines and remote organs [29,62]. Furthermore, numerous links have been established between ferroptosis and mitochondrial dysfunction, as evidenced by the disruption of ATP synthesis and elevation of ROS production, leading to aberrant iron transport and lipid peroxidation [63–65]. Several studies have demonstrated the association between ferroptosis and mitophagy. For instance, Lin et al. found that BNIP3-mediated and PINK1-PARK2-mediated mitophagy protected renal tubular epithelial cells against cisplatin-induced ferroptosis through the ROS/HO1/GPx4 axis [66]. Similarly, Bi et al. showed that Fundc1 interacted with GPx4 to promote hepatic ferroptosis and fibrotic injury through mitophagy-dependent mechanisms [67]. However, the potential interplay between mitophagy and ferroptosis in II/R-induced intestinal microvascular dysfunction remains inadequately understood. The present study utilized RNA sequencing to observe the differential expression of mitophagy and ferroptosis pathways in HUVECs cultured with or without NETs. Elevated intestinal microvascular endothelial ferroptosis was also observed in human II/R patients. The in vivo experimental findings demonstrated that NET formation exacerbated endothelial ferroptosis and microvascular dysfunction. However, the study also found that endothelial ferroptosis was alleviated by *Pad4* deficiency or ferroptosis inhibitor ferrostatin-1. In contrast, the administration of the ferroptosis activator erastin reversed the protective effect on the microvasculature and intensified ferroptosis. Furthermore, our findings indicated that the regulation of mitophagy impacted the level of ferroptosis, although the induction of ferroptosis did not influence the level of mitophagy. These outcomes provide evidence for a potential upstream and downstream association between mitophagy and ferroptosis in NET-induced microvascular damage after II/R.

The current investigation was constrained by certain limitations, namely, the potential existence of biological dissimilarities between HUVECs and intestinal endothelial cells and the possibility that the RNA-sequenced HUVECs might not comprehensively depict the alterations in gene expression in intestinal endothelial cells. Furthermore, our investigation demonstrated that the mitophagy process, dependent on Fundc1, significantly promoted ferroptosis in the intestinal endothelium, thereby leading to microvascular dysfunction. However, the possibility of other mechanisms underlying endothelial cell injury, such as oxidative stress, calcium overload, endoplasmic reticulum stress, and other forms of cell death induced by ischemia-reperfusion injury, cannot be disregarded. Additionally, our study explored the potential involvement of NETs in the advancement and exacerbation of intestinal microvascular damage during II/R. Small sample sizes may affect the current study on clinical specimens, resulting in potential selection bias and other influences. Thus, conducting further prospective studies or employing larger cohorts to corroborate our findings is imperative.

5. Conclusion

Our investigation demonstrated the involvement of NETs in the induction of intestinal microvascular dysfunction and vascular barrier injury resulting from II/R. The heightened infiltration of NETs was linked to mitophagy inhibition, mitochondrial dysfunction, and ferroptosis in the intestinal endothelium of both human patients and animals subjected to II/R. Furthermore, the mitigation of endothelial ferroptosis and intestinal vascular barrier injury caused by II/R was achieved through the restriction of NETs via neutrophil-specific *Pad4* deletion, which relieved the limitation of Fundc1-requiring mitophagy activation. Therefore, the present study may shed light on protecting the intestinal vascular barrier in II/R patients.

Funding

This work was supported by the National Natural Science Foundation of China (81770532, 82270587 and 51873087) and the Open Project of the State Key Laboratory of Trauma, Burn and Combined Injury, Third Military Medical University (SKLKF202103).

Author contributions

Chengnan Chu: Data curation; conceptualization; software; validation; investigation; visualization; methodology; writing – original draft. Xinyu Wang: Formal analysis; conceptualization; resources; data curation; investigation; writing – original draft. Chao Yang: Formal analysis; data curation; visualization; investigation; writing – original draft. Fang Chen: Resources; data curation; investigation. Lin Shi: Validation; investigation; methodology. Weiqi Xu: Software; formal analysis; visualization; methodology. Kai Wang: Data curation; investigation; methodology. Baochen Liu: Software; formal analysis. Chenyang Wang: Formal analysis; investigation. Dongping Sun: Project administration; funding acquisition; writing – review and editing. Weiwei Ding: Conceptualization; formal analysis; supervision; funding acquisition; visualization; project administration; writing – review and editing.

Declaration of competing interest

The authors declare no competing interests.

Data availability

Data will be made available on request.

Acknowledgements

We express our gratitude to Dr. Liping Jiang for providing assistance in the design of the study and the execution of the experiments. We would like to express our gratitude to the editorial team of Home for Researchers (www.home-for-researchers.com) for their valuable assistance in pattern diagram drawing.

Appendix A. Supplementary data

Supplementary data to this article can be found online at https://doi.org/10.1016/j.redox.2023.102906.

References

[1] F. Deng, Z.B. Lin, Q.S. Sun, Y. Min, Y. Zhang, Y. Chen, et al., The role of intestinal microbiota and its metabolites in intestinal and extraintestinal organ injury induced by intestinal ischemia reperfusion injury, Int. J. Biol. Sci. 18 (10) (2022) 3981–3992.

[2] J. Grootjans, K. Lenaerts, W.A. Buurman, C.H. Dejong, J.P. Derikx, Life and death at the mucosal-luminal interface: new perspectives on human intestinal ischemia-reperfusion, World J. Gastroenterol. 22 (9) (2016) 2760–2770.

[3] C. Tan, P.R. Norden, W. Yu, T. Liu, N. Ujiie, S.K. Lee, et al., Endothelial FOXC1 and FOXC2 promote intestinal regeneration after ischemia-reperfusion injury, EMBO Rep. (2023), e56030.

[4] Y.D. Feng, W. Ye, W. Tian, J.R. Meng, M. Zhang, Y. Sun, et al., Old targets, new strategy: apigenin-7-O-beta-d-(-6''-p-coumaroyl)-glucopyranoside prevents

endothelial ferroptosis and alleviates intestinal ischemia-reperfusion injury through HO-1 and MAO-B inhibition, Free Radic. Biol. Med. 184 (2022) 74–88.
[5] J.E. Schucht, P.J. Matheson, B.G. Harbrecht, L. Bond, S. Jones, K.J.M. Alkhateeb, et al., Plasma resuscitation with adjunctive peritoneal resuscitation reduces ischemic intestinal injury following hemorrhagic shock, J. Trauma Acute Care Surg. 89 (4) (2020) 649–657.
[6] Y.N. Zhang, Z.N. Chang, Z.M. Liu, S.H. Wen, Y.Q. Zhan, H.J. Lai, et al., Dexmedetomidine alleviates gut-vascular barrier damage and distant hepatic injury following intestinal ischemia/reperfusion injury in mice, Anesth. Analg. 134 (2) (2022) 419–431.
[7] V. Brinkmann, U. Reichard, C. Goosmann, B. Fauler, Y. Uhlemann, D.S. Weiss, et al., Neutrophil extracellular traps kill bacteria, Science 303 (5663) (2004) 1532–1535.
[8] G. Wigerblad, M.J. Kaplan, Neutrophil extracellular traps in systemic autoimmune and autoinflammatory diseases, Nat. Rev. Immunol. 23 (5) (2023) 274–288.
[9] M. Honda, P. Kubes, Neutrophils and neutrophil extracellular traps in the liver and gastrointestinal system, Nat. Rev. Gastroenterol. Hepatol. 15 (4) (2018) 206–221.
[10] F. Chen, C. Chu, X. Wang, C. Yang, Y. Deng, Z. Duan, et al., Hesperetin attenuates sepsis-induced intestinal barrier injury by regulating neutrophil extracellular trap formation via the ROS/autophagy signaling pathway, Food Funct. 14 (9) (2023) 4213–4227.
[11] Y. Cho, T.N. Bukong, D. Tornai, M. Babuta, I.S. Vlachos, E. Kanata, et al., Neutrophil extracellular traps contribute to liver damage and increase defective low-density neutrophils in alcohol-associated hepatitis, J. Hepatol. 78 (1) (2023) 28–44.
[12] R. Vats, T.W. Kaminski, T. Brzoska, J.A. Leech, E. Tutuncuoglu, O. Katoch, et al., Liver-to-lung microembolic NETs promote gasdermin D-dependent inflammatory lung injury in sickle cell disease, Blood 140 (9) (2022) 1020–1037.
[13] A. Blasco, M.J. Coronado, F. Hernandez-Terciado, P. Martin, A. Royuela, E. Ramil, et al., Assessment of neutrophil extracellular traps in coronary thrombus of a case series of patients with COVID-19 and myocardial infarction, JAMA Cardiol 6 (4) (2020) 1–6.
[14] H.H.L. Leung, J. Perdomo, Z. Ahmadi, S.S. Zheng, F.N. Rashid, A. Enjeti, et al., NETosis and thrombosis in vaccine-induced immune thrombotic thrombocytopenia, Nat. Commun. 13 (1) (2022) 5206.
[15] S. Sun, Z. Duan, X. Wang, C. Chu, C. Yang, F. Chen, et al., Neutrophil extracellular traps impair intestinal barrier functions in sepsis by regulating TLR9-mediated endoplasmic reticulum stress pathway, Cell Death Dis. 12 (6) (2021) 606.
[16] S. Wang, T. Xie, S. Sun, K. Wang, B. Liu, X. Wu, et al., DNase-1 treatment exerts protective effects in a rat model of intestinal ischemia-reperfusion injury, Sci. Rep. 8 (1) (2018), 17788.
[17] J.S. Harrington, S.W. Ryter, M. Plataki, D.R. Price, A.M.K. Choi, Mitochondria in health, disease, and ageing, Physiol. Rev. (2023).
[18] M.A. Eldeeb, R.A. Thomas, M.A. Ragheb, A. Fallahi, E.A. Fon, Mitochondrial quality control in health and in Parkinson's disease, Physiol. Rev. 102 (4) (2022) 1721–1755.
[19] L. Liu, K. Sakakibara, Q. Chen, K. Okamoto, Receptor-mediated mitophagy in yeast and mammalian systems, Cell Res. 24 (7) (2014) 787–795.
[20] Y. Liu, H. Zhang, Y. Liu, S. Zhang, P. Su, L. Wang, et al., Hypoxia-induced GPCPD1 depalmitoylation triggers mitophagy via regulating PRKN-mediated ubiquitination of VDAC1, Autophagy (2023) 1–21.
[21] H.O. Yazdani, E. Roy, A.J. Comerci, D.J. van der Windt, H. Zhang, H. Huang, et al., Neutrophil extracellular traps drive mitochondrial homeostasis in tumors to augment growth, Cancer Res. 79 (21) (2019) 5626–5639.
[22] P. Zhou, S. Zhang, M. Wang, J. Zhou, The induction mechanism of ferroptosis, necroptosis, and pyroptosis in inflammatory bowel disease, colorectal cancer, and intestinal injury, Biomolecules 13 (5) (2023).
[23] C. Xu, Z. Liu, J. Xiao, Ferroptosis: a double-edged sword in gastrointestinal disease, Int. J. Mol. Sci. 22 (22) (2021).
[24] N. Fefelova, S. Wongjaikam, S.H. Pamarthi, N. Siri-Angkul, T. Comollo, A. Kumari, et al., Deficiency of mitochondrial calcium uniporter abrogates iron overload-induced cardiac dysfunction by reducing ferroptosis, Basic Res. Cardiol. 118 (1) (2023) 21.
[25] J. Zhuang, B. Wang, H. Chen, K. Zhang, N. Li, N. Zhao, et al., Efficient NIR-II type-I AIE photosensitizer for mitochondria-targeted photodynamic therapy through synergistic apoptosis-ferroptosis, ACS Nano 17 (10) (2023) 9110–9125.
[26] B.R. Stockwell, X. Jiang, W. Gu, Emerging mechanisms and disease relevance of ferroptosis, Trends Cell Biol. 30 (6) (2020) 478–490.
[27] F.J. Bock, S.W.G. Tait, Mitochondria as multifaceted regulators of cell death, Nat. Rev. Mol. Cell Biol. 21 (2) (2020) 85–100.
[28] W. Gao, T. Zhang, H. Wu, Emerging pathological engagement of ferroptosis in gut diseases, Oxid. Med. Cell. Longev. 2021 (2021), 4246255.
[29] Y. Li, Y. Cao, J. Xiao, J. Shang, Q. Tan, F. Ping, et al., Inhibitor of apoptosis-stimulating protein of p53 inhibits ferroptosis and alleviates intestinal ischemia/reperfusion-induced acute lung injury, Cell Death Differ. 27 (9) (2020) 2635–2650.
[30] W. Ding, K. Wang, B. Liu, X. Fan, S. Wang, J. Cao, et al., Open abdomen improves survival in patients with peritonitis secondary to acute superior mesenteric artery occlusion, J. Clin. Gastroenterol. 51 (9) (2017) e77–e82.
[31] A.C. Silva Barbosa, D. Zhou, Y. Xie, Y.J. Choi, H.C. Tung, X. Chen, et al., Inhibition of estrogen sulfotransferase (SULT1E1/EST) ameliorates ischemic acute kidney injury in mice, J. Am. Soc. Nephrol. 31 (7) (2020) 1496–1508.
[32] J.A. Fels, G. Manfredi, Sex differences in ischemia/reperfusion injury: the role of mitochondrial permeability transition, Neurochem. Res. 44 (10) (2019) 2336–2345.
[33] E.O. Gubernatorova, E. Perez-Chanona, E.P. Koroleva, C. Jobin, A.V. Tumanov, Murine model of intestinal ischemia-reperfusion injury, J. Vis. Exp. 111 (2016).
[34] S. Van Coillie, E. Van San, I. Goetschalckx, B. Wiernicki, B. Mukhopadhyay, W. Tonnus, et al., Targeting ferroptosis protects against experimental (multi)organ dysfunction and death, Nat. Commun. 13 (1) (2022) 1046.
[35] Y. Zhang, Y. Yao, X. Qiu, G. Wang, Z. Hu, S. Chen, et al., Listeria hijacks host mitophagy through a novel mitophagy receptor to evade killing, Nat. Immunol. 20 (4) (2019) 433–446.
[36] M. Zhang, S. Cui, B. Mao, Q. Zhang, J. Zhao, X. Tang, et al., Urolithin A produced by novel microbial fermentation possesses anti-aging effects by improving mitophagy and reducing reactive oxygen species in Caenorhabditis elegans, J. Agric. Food Chem. 71 (16) (2023) 6348–6357.
[37] J.R. Huang, M.H. Zhang, Y.J. Chen, Y.L. Sun, Z.M. Gao, Z.J. Li, et al., Urolithin A ameliorates obesity-induced metabolic cardiomyopathy in mice via mitophagy activation, Acta Pharmacol. Sin. 44 (2) (2023) 321–331.
[38] C.J. Chiu, A.H. McArdle, R. Brown, H.J. Scott, F.N. Gurd, Intestinal mucosal lesion in low-flow states. I. A morphological, hemodynamic, and metabolic reappraisal, Arch. Surg. 101 (4) (1970) 478–483.
[39] S. Najmeh, J. Cools-Lartigue, B. Giannias, J. Spicer, L.E. Ferri, Simplified human neutrophil extracellular traps (NETs) isolation and handling, J. Vis. Exp. 98 (2015).
[40] S. Polyak, A. Mach, S. Porvasnik, L. Dixon, T. Conlon, K.E. Erger, et al., Identification of adeno-associated viral vectors suitable for intestinal gene delivery and modulation of experimental colitis, Am. J. Physiol. Gastrointest. Liver Physiol. 302 (3) (2012) G296–G308.
[41] Y. Fang, Z.Y. Shen, Y.Z. Zhan, X.C. Feng, K.L. Chen, Y.S. Li, et al., CD36 inhibits beta-catenin/c-myc-mediated glycolysis through ubiquitination of GPC4 to repress colorectal tumorigenesis, Nat. Commun. 10 (1) (2019) 3981.
[42] H. Zhou, P. Zhu, J. Guo, N. Hu, S. Wang, D. Li, et al., Ripk3 induces mitochondrial apoptosis via inhibition of FUNDC1 mitophagy in cardiac IR injury, Redox Biol. 13 (2017) 498–507.
[43] S. Li, Y. Zhou, X. Gu, X. Zhang, Z. Jia, NLRX1/FUNDC1/NIPSNAP1-2 axis regulates mitophagy and alleviates intestinal ischaemia/reperfusion injury, Cell Prolif. 54 (3) (2021), e12986.
[44] S. Liao, J. Luo, T. Kadier, K. Ding, R. Chen, Q. Meng, Mitochondrial DNA release contributes to intestinal ischemia/reperfusion injury, Front. Pharmacol. 13 (2022), 854994.
[45] D.N. Granger, L. Holm, P. Kvietys, The gastrointestinal circulation: physiology and pathophysiology, Compr. Physiol. 5 (3) (2015) 1541–1583.
[46] G. Li, S. Wang, Z. Fan, Oxidative stress in intestinal ischemia-reperfusion, Front. Med. 8 (2021), 750731.
[47] M. Honda, M. Kadohisa, D. Yoshii, Y. Komohara, T. Hibi, Intravital imaging of immune responses in intestinal inflammation, Inflamm. Regen. 43 (1) (2023) 9.
[48] A. Bosi, D. Banfi, M. Bistoletti, L.M. Catizzone, A.M. Chiaravalli, P. Moretto, et al., Hyaluronan regulates neuronal and immune function in the rat small intestine and colonic microbiota after ischemic/reperfusion injury, Cells 11 (21) (2022).
[49] A. Horowitz, S.D. Chanez-Paredes, X. Haest, J.R. Turner, Paracellular permeability and tight junction regulation in gut health and disease, Nat. Rev. Gastroenterol. Hepatol. (2023) 1–16.
[50] C. Pellegrini, M. Fornai, V. D'Antongiovanni, L. Antonioli, N. Bernardini, P. Derkinderen, The intestinal barrier in disorders of the central nervous system, Lancet Gastroenterol Hepatol 8 (1) (2023) 66–80.
[51] C.R. Behem, M.F. Graessler, T. Friedheim, R. Kluttig, H.O. Pinnschmidt, A. Dupree, et al., The use of pulse pressure variation for predicting impairment of microcirculatory blood flow, Sci. Rep. 11 (1) (2021) 9215.
[52] J. Yang, M. Meng, C. Pan, L. Qian, Y. Sun, H. Shi, et al., Intravoxel incoherent motion and dynamic contrast-enhanced magnetic resonance imaging to early detect tissue injury and microcirculation alteration in hepatic injury induced by intestinal ischemia-reperfusion in a rat model, J. Magn. Reson. Imag. 54 (3) (2021) 751–760.
[53] Z. Duan, S. Sun, C. Qu, K. Wang, F. Chen, X. Wang, et al., Neutrophil extracellular trap formation index predicts occurrences of deep surgical site infection after laparotomy, Ann. Transl. Med. 9 (17) (2021) 1373.
[54] C. Zhang, X. Gao, M. Li, X. Yu, F. Huang, Y. Wang, et al., The role of mitochondrial quality surveillance in skin aging: focus on mitochondrial dynamics, biogenesis and mitophagy, Ageing Res. Rev. 87 (2023), 101917.
[55] M.Y.W. Ng, T. Wai, A. Simonsen, Quality control of the mitochondrion, Dev. Cell 56 (7) (2021) 881–905.
[56] M. Chen, G. Zhong, M. Liu, H. He, J. Zhou, J. Chen, et al., Integrating network analysis and experimental validation to reveal the mitophagy-associated mechanism of Yiqi Huoxue (YQHX) prescription in the treatment of myocardial ischemia/reperfusion injury, Pharmacol. Res. 189 (2023), 106682.
[57] A.R. Bland, F.M. Payne, J.C. Ashton, T. Jamialahmadi, A. Sahebkar, The cardioprotective actions of statins in targeting mitochondrial dysfunction associated with myocardial ischaemia-reperfusion injury, Pharmacol. Res. 175 (2022), 105986.
[58] L. Ma, K. Li, W. Wei, J. Zhou, Z. Li, T. Zhang, et al., Exercise protects aged mice against coronary endothelial senescence via FUNDC1-dependent mitophagy, Redox Biol. 62 (2023), 102693.

[59] Y. Lim, B. Berry, S. Viteri, M. McCall, E.C. Park, C. Rongo, et al., FNDC-1-mediated mitophagy and ATFS-1 coordinate to protect against hypoxia-reoxygenation, Autophagy 17 (11) (2021) 3389–3401.
[60] H. Liu, C. Zang, F. Yuan, C. Ju, M. Shang, J. Ning, et al., The role of FUNDC1 in mitophagy, mitochondrial dynamics and human diseases, Biochem. Pharmacol. 197 (2022), 114891.
[61] Y.L. Qi, H.R. Wang, L.L. Chen, Y.T. Duan, S.Y. Yang, H.L. Zhu, Recent advances in small-molecule fluorescent probes for studying ferroptosis, Chem. Soc. Rev. 51 (18) (2022) 7752–7778.
[62] Y. Li, D. Feng, Z. Wang, Y. Zhao, R. Sun, D. Tian, et al., Ischemia-induced ACSL4 activation contributes to ferroptosis-mediated tissue injury in intestinal ischemia/reperfusion, Cell Death Differ. 26 (11) (2019) 2284–2299.
[63] C. Liu, Z. Li, B. Li, W. Liu, S. Zhang, K. Qiu, et al., Relationship between ferroptosis and mitophagy in cardiac ischemia reperfusion injury: a mini-review, PeerJ 11 (2023), e14952.
[64] S. Granata, V. Votrico, F. Spadaccino, V. Catalano, G.S. Netti, E. Ranieri, et al., Oxidative stress and ischemia/reperfusion injury in kidney transplantation: focus on ferroptosis, mitophagy and new antioxidants, Antioxidants 11 (4) (2022).
[65] W. Li, Z. Xiang, Y. Xing, S. Li, S. Shi, Mitochondria bridge HIF signaling and ferroptosis blockage in acute kidney injury, Cell Death Dis. 13 (4) (2022) 308.
[66] Q. Lin, S. Li, H. Jin, H. Cai, X. Zhu, Y. Yang, et al., Mitophagy alleviates cisplatin-induced renal tubular epithelial cell ferroptosis through ROS/HO-1/GPX4 axis, Int. J. Biol. Sci. 19 (4) (2023) 1192–1210.
[67] Y. Bi, S. Liu, X. Qin, M. Abudureyimu, L. Wang, R. Zou, et al., FUNDC1 interacts with GPx4 to govern hepatic ferroptosis and fibrotic injury through a mitophagy-dependent manner, J. Adv. Res. (2023).